Mesenchymal Stem Cell-Derived Exosomes as Drug Carriers for Delivering miRNA-29b to Ameliorate Inflammation in Corneal Injury Via Activating Autophagy

Jinghua Liu,[1,2] Juan Gao,[2] Ping Lu,[2] Yuchuan Wang,[2] Shulei Xing,[3] Yarong Yan,[3] Ruifang Han,[2] Peng Hao,[2] and Xuan Li[1–3]

[1]School of Medicine, Nankai University, Tianjin, China; Nankai University Affiliated Eye Hospital, Tianjin, China
[2]Tianjin Eye Hospital, Tianjin Key Lab of Ophthalmology and Vision Science, Tianjin Eye Institute, Tianjin, China
[3]Clinical College of Ophthalmology, Tianjin Medical University, Tianjin, China

Correspondence: Xuan Li, Tianjin Eye Hospital, Tianjin Key Lab of Ophthalmology and Vision Science, Tianjin Eye Institute, 4 Gansu Rd., Heping District, Tianjin, P.r.c 300020, China;
xuanli08@yahoo.com.

Received: December 18, 2023
Accepted: May 17, 2024
Published: June 10, 2024

Citation: Liu J, Gao J, Lu P, et al. Mesenchymal stem cell-derived exosomes as drug carriers for delivering miRNA-29b to ameliorate inflammation in corneal injury via activating autophagy. *Invest Ophthalmol Vis Sci.* 2024;65(6):16. https://doi.org/10.1167/iovs.65.6.16

Purpose. Corneal injury (CI) resulting in corneal opacity remains a clinical challenge. Exosomes (Exos) derived from bone marrow mesenchymal stem cells (BMSCs) have been proven effective in repairing various tissue injuries and are also considered excellent drug carriers due to their biological properties. Recently, microRNA-29b (miR-29b) was found to play an important role in the autophagy regulation which correlates with cell inflammation and fibrosis. However, the effects of miR-29b and autophagy on CI remain unclear. To find better treatments for CI, we used Exos to carry miR-29b and investigated its effects in the treatment of CI.

Methods. BMSCs were transfected with miR-29b-3p agomir/antagomir and negative controls (NCs) to obtain Exos-29b-ago, Exos-29b-anta, and Exos-NC. C57BL/6J mice that underwent CI surgeries were treated with Exos-29b-ago, Exos-29b-anta, Exos-NC, or PBS. The autophagy, inflammation, and fibrosis of the cornea were estimated by slit-lamp, hematoxylin and eosin (H&E) staining, immunofluorescence, RT–qPCR, and Western blot. The effects of miR-29b-3p on autophagy and inflammation in immortalized human corneal epithelial cells (iHCECs) were also investigated.

Results. Compared to PBS, Exos-29b-ago, Exos-29b-anta, and Exos-NC all could ameliorate corneal inflammation and fibrosis. However, Exos-29b-ago, which accumulated a large amount of miR-29b-3p, exerted excellent potency via autophagy activation by inhibiting the PI3K/AKT/mTOR pathway and further inhibited corneal inflammation via the mTOR/NF-κB/IL-1β pathway. After Exos-29b-ago treatment, the expressions of collagen type III, α-smooth muscle actin, fibronectin, and vimentin were significantly decreased than in other groups. In addition, overexpression of miR-29b-3p prevented iHCECs from autophagy impairment and inflammatory injury.

Conclusions. Exos from BMSCs carrying miR-29b-3p can significantly improve the therapeutic effect on CI via activating autophagy and further inhibiting corneal inflammation and fibrosis.

Keywords: exosome, microRNA-29b, autophagy, PI3K/AKT/mTOR pathway, corneal injury (CI), corneal fibrosis

The cornea is an important component of the refractive elements of the eye and is part of the outer wall of the eye. Various corneal injuries (CIs) induce corneal inflammation and fibrosis, affect the corneal epithelium and stroma, and damage the transparency and integrity of the cornea, leading to corneal neovascularization, corneal fibrosis, scar formation, and even complete blindness. The regeneration and stability of the corneal epithelium and stroma are crucial for preventing injuries to the deeper layers of the cornea. However, it is still a clinical challenge.

Autophagy, a process of autophagosome and autolysosome formation and content degradation, has proven to be extremely important for intracellular self-renewal and material metabolism.[1] During nutrient deprivation and stress conditions, autophagy is activated in cells to recycle the degradation products, or remove the redundant organelles and the misfolded proteins. Therefore, autophagy is crucial for maintaining cellular homeostasis and energy balance. Autophagy can be classified into three distinct categories: macro-autophagy, micro-autophagy, and chaperone-mediated autophagy. Macro-autophagy is generally referred to as autophagy.[2] The process of autophagosome formation in the autophagy activation involves three main steps, including (1) vesicle nucleation (formation), (2) vesicle elongation (expansion), and (3) vesicle completion (fusion). It is a highly conserved process. During the process, at least 31 autophagy-related proteins (Atg) are involved.[3] Autophagy abnormalities are closely related to many diseases, such as

tumors,[4] diabetes,[5] and hepatic injury.[6] In addition, activation of autophagy protects human retinal pigment epithelium cells from blue light-induced damage.[7] Autophagy activation could reduce corneal inflammation in a mice model of fungal keratitis.[8] Therefore, the regulation of autophagy could play a critical role during the process of corneal wound healing.

MicroRNAs (miR), a class of highly conserved, small endogenous noncoding RNA molecules, negatively regulate gene expression at the post-transcriptional level.[9] It has been confirmed that microRNA-29b (miR-29b) prevents or inhibits fibrosis in many tissues and organs by targeting extracellular matrix (ECM)-related genes.[10–12] A study indicated that cardiac fibrosis induced by chronic angiotensin II infusion resulted in a significant downregulation of miR-29b in mice.[13] Another study confirmed that overexpression of miR-29b in human corneal endothelial cells led to a decrease in ECM protein production in the Descemet membrane.[14] Therefore, miR-29b, as a potency and a kind of anti-fibrosis agent in CI treatment, has still been in the spotlight. However, it has also been reported that silencing miR–29b–3p expression protects human trabecular meshwork cells against oxidative injury via upregulation of E3 ubiquitin–protein ligase RNF138 to activate the ERK pathway.[15] Recently, with the development of researches about the target genes and target signaling pathways of miRNA-29b, more and more regulatory functions of miR-29b have been taking more attention. It is noteworthy that phosphoinositide 3-kinase (PI3K) and protein kinase B (AKT), as the target genes of miR-29b, play important roles in various physiologic processes, including autophagy. For example, through targeting PI3K(p85α), miR-29b agomir inhibited the PI3K/AKT/mTOR (mammalian target of rapamycin) signaling pathway and activated autophagy in muscle atrophy mouse and C2C12 myotubes.[16] MiR-29b-3p plays a significant role in motor function improvement and nerve function repair in spinal cord injury rats via inhibiting AKT and mTOR related signaling pathway.[17] However, the effect and mechanism of miR-29b on autophagy regulation in CI have not been well revealed.

Exosomes (Exos) or small extracellular vesicles are cell-derived nanovesicles encapsulating proteins, mRNAs, miRs, and lipids that are involved in the intercellular transportation of materials. Consequently, the characteristic make of Exos can be used as drug-delivery nanocarriers.[18,19] Compared with liposomes or other synthetic polymer based drug carriers, Exos has the following advantages: (1) Exos contain transmembrane and membrane-anchored proteins that enhance endocytosis and promote payload delivery[20]; (2) Exos have higher biocompatibility and lower toxicity[21]; and (3) Exos can also diffuse to the blood and even cross the blood–brain barrier.[22] Bone marrow mesenchymal stem cells (BMSCs) are easily obtained and are considered to be the most effective exosome-producing cells.[23] Exos derived from BMSCs retain the repair capacity and have low immunogenicity and, therefore, it has broad application prospects.[24] More and more studies have proved that miRNA is the one of the most effective contents in Exos derived from BMSCs. For instance, research has demonstrated that Exos derived from BMSCs successfully delivered their cargo into inner retinal layers and the effects were reliant on miRNA.[25] In addition, the results of research showed that exosomal microRNA-21 from BMSCs serve as a therapeutic for retinal degeneration.[26]

In the present study, we explore the effect and mechanisms of miR-29b-3p carried by Exos from BMSCs transfected with miR-29b-3p agomir (Exos-29b-ago) in both vivo and vitro. The results showed that Exos-29b-ago ameliorate corneal inflammation and fibrosis by activating autophagy via inhibiting the PI3K/AKT/mTOR pathway. It suggested that Exos-29b-ago might represent a novel therapeutic approach for corneal inflammation and corneal fibrosis during the corneal wound healing process.

Materials and Methods

Cell Culture and Transfection

Primary Bone Marrow Mesenchymal Stem Cells Culture. Primary BMSCs were derived from bone marrow collected from the femurs and tibias of 3- to 5-week-old male C57BL/6J mice (Beijing HFK Bioscience Co. Ltd., Beijing, China) by direct adherence of bone marrow suspension. The BMSCs were cultured in bone marrow mesenchymal stem cell culture medium (Cyagen, USA) with 10% fetal bovine serum (FBS; Cyagen, USA) and 1% penicillin and streptomycin (v/v) at 37°C with 5% CO_2. To identify the cells, the expression levels of CD34 (Invitrogen, CA, USA; 11-0341-82), CD45 (Invitrogen, CA, 12-0451-82), CD90 (Invitrogen, CA, 45-0900-82), CD105 (Invitrogen, CA, 25-1051-82), and CD44 (Invitrogen, CA, 17-0441-82) in the BMSCs at passage 3-4 were analyzed using flow cytometry (BD AriaIII).

Immortalized Human Corneal Epithelial Cell Line Culture. The SV40 immortalized human corneal epithelial cell (iHCEC) line provided by Professor Liu Zuguo (Xiamen University) through the RIKEN Cell Bank (RCB1384, Tsukuba, Japan) was cultured in DMEM/F12 (Gibco, USA) supplemented with 6% FBS (Gibco, USA), 7 µg/mL insulin (Sigma–Aldrich), 7 ng/mL epithelium growth factor (Gibco, USA), and 1% penicillin and streptomycin (v/v) at 37°C with 5% CO_2. The iHCECs from the third to fifth passage were used for the subsequent experiments.

BMSCs and iHCECs Transfection

The miR-29b-3p agomir, antagomir and their respective negative controls (NCs) were synthesized and purified by Genepharma Co., Ltd. (Shanghai, China). The agomir of miR-29b-3p was double stranded with the following sequence: sense 5′-UAGCACCAUUUGAAAUCAGUGUU-3′ and antisense 5′-CACUGAUUUCAAAUGGUGCUAUU-3′. Agomir NC: sense 5′-UUCUCCGAACGUGUCACGUTT-3′ and antisense 5′-ACGUGACACGUUCGGAGAATT-3′. The miR-29b-3p antagomir was single stranded with the following sequence: 5′-AACACUGAUUUCAAAUGGUGCUA-3′. Antagomir NC: 5′-CAGUACUUUUGUGUAGUACAA-3′. BMSCs were transfected with miR-29b-3p agomir/ antagomir or NCs in DMEM/F12 without antibiotics or FBS. Twenty-four hours after transfection, new bone marrow mesenchymal stem cell culture medium was added. Then, the culture medium was collected to extract the exosomes (Exos-29b-ago, Exos-29b-anta, and Exos-NC). The iHCECs were transfected with miR-29b-3p agomir/antagomir or NC using Lipofectamine 3000 Transfection Reagent (Invitrogen, CA) according to the manufacturer's instructions. To induce iHCEC injury in vitro, cells were incubated with 200 ng/mL LPS (lipopolysaccharide) for 24 hours. Real-time quantitative PCR (RT-qPCR) was used to evaluate the effect of transfection.

Investigative Ophthalmology & Visual Science

Isolation, Identification, and Quantification of BMSC-Exos

The culture medium of the BMSCs was collected and filtered. Differential ultracentrifugation was used to purify the exosomes derived from BMSCs (BMSC-Exos) as in previous protocols.[27] A brief description is as follows: first, the supernatant was first centrifuged at 10,000 × *g* for 30 minutes at 4°C to remove the dead cells and cell debris. Then, the supernatant was centrifuged at 100,000 × *g* for 70 minutes at 4°C to get the precipitates. To purify the exosomes, the precipitates were washed with phosphate buffered saline (PBS) by centrifugation at 100,000 × *g* for 70 minutes at 4°C. Finally, the supernatant was collected and resuspended in 50 to 100 µL of PBS. The exosomes were characterized by transmission electron microscopy (TEM) and nanoparticle tracking analysis (NTA). The expressions of the protein markers TSG101 (Abcam, USA, Ab125011), Hsp70 (Abcam, USA, ab181606), and calnexin (Abcam, USA, ab133615) were detected using Western blot assays.

Uptake of the Exos

BMSCs-Exos after transfection with miR-29b-3p agomir (Exos-29b-ago) and control Exos (Exos-NC) were both labeled with 1 µM Dil (Invitrogen, CA). Briefly, Exos-29b-ago and Exos-NC were mixed with 1 µM Dil and incubated for 1 hour at 37°C with regular mixing. Then, the labeled suspensions were centrifuged at 100,000 × *g* for 70 minues at 4°C and washed again with PBS. Then, the Exos were resuspended in PBS. The Exos-NC without Dil-labele was set as Ctrl. In vitro, 1×10^8/µL Dil-labeled Exos were cocultured with iHCECs for 12 hours, and then the cells were washed with cell culture medium without FBS and observed by fluorescence microscopy. In vivo, male C57BL/6 J mice aged 6 to 8 weeks were anesthetized using pentobarbital sodium solution (70 mg/kg) and proparacaine hydrochloride eye drops (Santen, Japan). The corneal surface was scratched with an AlgerBrush II corneal remover (Alger, USA). The Dil-labeled Exos were applied topically to the eye, 1×10^8/µL per hour per eye. After 12 hours, the mice were euthanized, and their whole corneas were removed immediately to make a stretched cornea preparation and were observed by fluorescence microscopy.

CI Model of C57BL/6J Mice

The animal procedures were approved by the Laboratory Animal Ethics Committee of Nankai Hospital (Approval No. NKYY-DWLL-2023-052). Experiments were conducted in accordance with the ARVO Statement for the Use of Animals in Ophthalmic and Vision Research. Male C57BL/6 J mice aged 6 to 8 weeks (Beijing HFK Bioscience Co. Ltd., Beijing, China) were applied to established animal CI model as described previously.[28] A brief description is as follows. Mice were checked under a slit-lamp, and those with anterior segmental lesions were excluded. Animals were maintained in a standard condition where a 12-hour light/dark cycle at 22°C to 24°C with 45% to 50% humidity is available. Mice were randomly divided into 5 groups ($n = 6$): normal (N), PBS, Exos-NC, Exos-29b-ago, and Exos-29b-anta. The process of CI surgery is briefly described as follows: mice were anesthetized using pentobarbital sodium solution (70 mg/kg) and proparacaine hydrochloride eye drops (Santen, Japan). The whole corneal epithelium and superficial stroma were scratched with AlgerBrush II corneal remover after they were marked with a 2.5 mm trephine. Topical application of Exos-29b-ago (1×10^8/µL), Exos-29b-anta (1×10^8/µL), and Exos-NC (1×10^8/µL) or PBS was administered according to the group, 3 times a day, 5 µL per eye, within 7 days after corneal injury. Then, the administration pathways of Exos-29b-ago, (1×10^8/µL) Exos-NC (1×10^8/µL) or PBS were changed to subconjunctival injection once every 2 days, 5 µL per eye, until 14 days after corneal injury.

Evaluation of Corneal Inflammatory Index, Haze Grade Scores, and Fluorescein Staining

After anesthesia, the corneas of CI mice in all groups were observed through a slit lamp under bright light and graded based on the corneal inflammatory index (at 3 days after injury) and corneal haze grading method (at 1 week and 2 weeks after injury). (1) The inflammatory index was analyzed as previously described,[29] briefly, grading followed three aspects (from slight to severe stages) as follows: ciliary hyperemia (0–3), central corneal edema (0–3), and peripheral corneal edema (0–3). The inflammatory index = total score (0–9) divided by a factor of 9; (2) Haze grade scores were as follows[30]: completely clear cornea (grade 0), cornea haze with iris details visible (grade 1), corneal opacities with mild obscuration of iris details (grade 2), corneal opacities with moderate obscuration of iris details (grade 3), and complete corneal opacification with iris details and pupil invisible (grade 4). Three independent ophthalmologists observed the corneal inflammatory index and haze grade in a blinded manner. Corneal defects were observed under cobalt blue light from a slit lamp, and fluorescein sodium (0.1%; Tianjin Jingming, China) was applied to the corneal epithelium. The area of corneal epithelial defects was quantified by using ImageJ (version 2.3.0).

Transmission Electron Microscopy

After the mice were euthanized, the eyeballs were taken and immediately fixed in 2.5% glutaraldehyde. After fixation for 24 hours at room temperature, the eyeballs of all groups were dehydrated with ethanol and acetone and embedded in epoxy resin. Ultrathin sagittal sections (60 nm) were sliced using an Ultracut ultramicrotome (Ultracut, Leica) and placed on slot grids. Finally, the sections were counterstained with 1% uranium acetate and observed through a transmission electron microscope (TEM).

Hematoxylin and eosin staining and immunohistochemistry Staining

After the mice were euthanized, the eyeballs were taken and immediately fixed in 4% paraformaldehyde. After fixation for 24 hours at room temperature, the eyeballs underwent gradient dehydration and were embedded in paraffin. Then, samples from all groups were taken for sectioning, followed by hematoxylin and eosin (H&E) staining and immunohistochemistry staining. Heat-induced antigen retrieval was performed by using EDTA (pH 8.0; Solarbio, China). To reduce the nonspecific background staining caused by endogenous peroxidase, the slices were incubated in a hydrogen peroxide block for 10 to 15 minutes at room temperature. Goat serum (5%; Gibco, USA) was added drop-

wise to the tissue and incubated at room temperature for 30 minutes to block nonspecific background staining. Then, anti-α-smooth muscle actin (α-SMA, Abcam, USA, ab124964) was incubated overnight at 4°C. The Envision horseradish peroxidase system (Gene Tech, Shanghai, China) was added dropwise and incubated at room temperature for 30 minutes. Then, 25 µL of 3,3′-diaminobenzidine (DAB; Gene Tech, Shanghai, China) was added dropwise to the slice and incubated for 3 to 15 minutes. Finally, after nuclear hematoxylin re-staining, the tissue sections were visualized, and images were captured with a microscope (Nikon DS-Ri2, Japan).

Immunofluorescence

After the mice were euthanized, the eyeballs were removed and embedded in O.C.T. compound (Sakura, USA). The specimens were sliced into 10 µm sections immediately after O.C.T. compound was frozen at -20°C. Next, the samples were fixed with 0.4% paraformaldehyde (15 minutes), blocked with 5% goat serum (30 minutes at room temperature), and incubated with primary antibodies overnight at 4°C. The antibodies were as follows: anti-collagen type III alpha 1 chain (COLIII, ABclonal, China, A0817), anti-fibronectin (FN1; Abcam, USA, ab23750), and anti-vimentin (Vim; Abcam, USA, ab92547). After washing with PBS three times, tissue sections were incubated with Alexa Fluor-conjugated secondary antibodies (Alexa Fluor 488-conjugated goat anti-rabbit; Thermo Fisher Scientific, USA). Finally, the slides were incubated with DAPI and mounted with antifade mounting medium. The tissue sections were visualized, and images were captured with a laser scanning confocal microscope (TCS SP8; Leica, Germany).

Cell Cycle Assay

The iHCECs were incubated with PI/RNase staining working solution (Dojindo Laboratories, Japan) as previously described. Briefly, harvested iHCECs were washed with PBS. A total of 1×10^6 iHCECs were added to 0.5 mL working solution (25 µL PI solution and 2.5 µL RNase solution were added to 500 µL assay buffer) and cultured at 4°C in the dark for 30 minutes. After vortex oscillation dispersed the cells, the cells were cultured at 37°C in the dark for 30 minutes. The cells were dispersed by vortex oscillation, filtered with a nylon mesh (300 mesh) to remove cell clumps from the sample, and detected by flow cytometry (BD AriaIII).

Cell Viability Assay (CCK-8)

The proliferation of iHCECs after transfection with miR-29b-3p agomir/antagomir or their NC was quantitatively evaluated by the cell count kit (CCK-8; Dojindo Laboratories, Japan). The iHCECs were inoculated in 96-well culture plates at 1-2 $\times$ 10^3 per well. After transfection with miR-29b-3p agomir/antagomir or NC, the cell medium was replaced with DMEMF/12 containing 10% CCK-8 solution. After 1 hour of incubation at 37°C and 5% CO_2, the OD values of each well were detected at a wavelength of 450 nm using an enzyme-linked immunosorbent assay.

Cell Migration Assay

The culture inserts were placed in 24-well plates. Then, 70 µL of cell suspension (1-2 $\times$ 10^4/mL) was added to each well of a 2-well culture insert (Ibidi, Germany) and placed in an incubator for cultivation at 37°C with 5% CO_2. After cell adhesion, sterilized tweezers were used to gently remove the culture insert. PBS was used to wash the cells to remove the floating cells. Then, serum-free medium was added for cultivation. Images of the cells were taken every 30 minutes, and the experimental results were analyzed using a Cytation 5 Cell Imaging Multimode Reader (Bio Tek, USA). The area of iHCECs at every time point was further processed by the following formula: Area of iHCECs = Sum $\text{Area}_{\text{time point}}$ − Sum $\text{Area}_{0\ \text{hour}}$.

Table. Sequence of Primers for RT-qPCR

Gene	Species	Direction	Primer Sequence 5′→3′
GAPDH	Human	Forward	TGCCCTCAACGACCACTTTG
		Reverse	CTGGTGGTCCAGGGGTCTTA
IL-1β	Human	Forward	TCATACCAAGGAGAAGTAATAAGCC
		Reverse	ACCAAAGAAGTACAGCGCCAT
β-actin	Mouse	Forward	GATTACTGCTCTGGCTCCTAGC
		Reverse	GACTCATCGTACTCCTGCTTGC
IL-1β	Mouse	Forward	GCAACTGTTCCTGAACTCAACT
		Reverse	ATCTTTTGGGGTCCGTCAACT
COL3A1	Mouse	Forward	AAGGCTGCAAGATGGATGCT
		Reverse	GTGCTTACGTGGGACAGTCA
α-SMA	Mouse	Forward	CAGCGGGCATCCACGAAAC
		Reverse	CCTGACAGGACGTTGTTAGCAT
FN1	Mouse	Forward	ACCATCTACGTCATTGCCCTG
		Reverse	ACCAGTTGGGGAAGCTCATC
Vim	Mouse	Forward	TTCTCTGGCACGTCTTGACC
		Reverse	GCTTGGAAACGTCCACATCG
MiR-29b-3p	Mouse	Forward	CTGCCGTAGCACCATTTGA
	Mouse	Reverse	TATCCTTGTTCACGACTCCTTCAC
	Human	Forward	CTGCCGTAGCACCATTTGA
	Human	Reverse	TATCCTTGTTCACGACTCCTTCAC
U6		Forward	GCTTCGGCAGCACATATACTAAAAT
		Reverse	CGCTTCAGAATTTGCGTGTCAT

Real-Time Quantitative PCR

Total RNA was purified using a total RNA purification kit (SBS, Beijing, China). The concentration of total RNA was quantified by spectrophotometry, and cDNA was synthesized with M-MLV reverse transcriptase (Promega, USA). Real-time quantitative polymerase chain reaction (RT–qPCR) was performed with SYBR Primix Ex Taq (Takara, Japan) and the StepOnePlus Real-Time PCR system (Applied Biosystems, USA) according to the manufacturer's protocol. Glyceraldehyde 3-phosphate dehydrogenase (GAPDH) was used as a control. To evaluate the expression of miR-29b-3p, cDNA of miR-29b-3p was synthesized with specified reverse transcription primers (Genepharma, China) and M-MLV reverse transcriptase (Promega, USA). The small nuclear RNA U6 (RNU6) was used as a control for miR-29b-3p. Specific miR stem–loop reverse transcription was performed using a microRNA first-strand cDNA synthesis kit (Vazyme, China). RT–qPCR was performed by using SYBR Green Master Mix (Vazyme). The primer sequences are shown in the Table. The relative quantification of miR levels was calculated using the $2^{-\Delta\Delta Ct}$ method.

Western Blotting

Corneal tissue and iHCECs were lysed in RIPA buffer (Beyotime Institute of Biotechnology, China) for 30 minutes, and proteins were harvested after centrifugation. The protein concentration was determined using a BCA protein

Investigative Ophthalmology & Visual Science

assay kit (Thermo, USA). Proteins (30 µg per lane) were separated by SDS–PAGE and transferred to a polyvinylidene difluoride (PVDF) membrane (Millipore, USA). The membranes were blocked in 5% skim milk (Biotopped, China) in PBS containing 0.1% Tween-20 for 2 hours and then incubated with ULK1 (Cell Signaling Technology, USA, 8054S), p-ULK1 (Cell Signaling Technology, USA, 5869), p62 (Abmart, China, T55546), LC3B I and II (Abcam, USA, ab192890), PI3 kinase p85 alpha (PI3K, Abcam, USA, ab191606), p-PI3K (Abcam, USA, ab182651), AKT (Abcam, USA, ab179463), p-AKT (Abcam, USA, ab192623), p-mTOR (Abmart, China, T56571), mTOR (Abcam, USA, ab134903), NF-κB-p65 (Cell Signaling Technology, USA, 3033S), IL-1β (Abcam, USA, ab9722), and GAPDH (Abcam, USA, ab181602) at 4°C overnight. After 1.5 hours of incubation with goat anti-rabbit IgG HRP (Abcam, USA, ab6721), the protein bands were detected using chemiluminescence reagents (Beyotime, China). The immunoreactive bands were quantified by densitometry through ImageJ (version 2.3.0).

Statistical Analysis

The results are presented as the means ± standard deviations (SDs). One-way ANOVA was performed to compare multiple groups, followed by Bonferroni's post hoc test. The differences between the 2 groups were performed using unpaired 2-tailed Student's *t*-tests using SPSS 24.0 (IBM, USA). The differences were considered statistically significant at $P < 0.05$.

Results

The Target Gene and Signaling Pathway of miR-29b-3p

To clarify the potential biological regulatory role of miR-29b-3p, we searched the bioinformatic tools TargetScan and miRDB to explore the potential target genes of miR-29b-3p and performed Kyoto Encyclopedia of Genes and Genomes (KEGG) pathway enrichment analysis based on the search results. The results showed that miR-29b-3p can target PI3K (p85α; Fig. 1A). Furthermore, it might inhibit the PI3K/AKT pathway (Fig. 1B), and further play an important role in autophagy via mTOR, a downstream gene of the PI3K/AKT pathway and a key protein in autophagy regulation.

Characterizations of BMSCs and BMSC-Exos

First, the surface markers of BMSCs passaged to the third to fourth generations were detected by flow cytometry. The results showed that the expressions of CD90, CD105, and CD44 were positive in BMSCs, whereas the expressions of CD34 and CD45 were negative (Fig. 1C). The results showed that we successfully extracted BMSCs with acceptable purity. Then, we collected the BMSCs culture medium supernatants from the first to the third days after transfection and extracted extracellular vesicles by ultracentrifugation. The extracted precipitates were detected through TEM, NTA, and Western blot. The results showed that the extracellular vesicles obtained by centrifugation were disc shaped (Fig. 1D) and approximately 100 nm in size (Fig. 1E). The Western blot results showed positive expression of Hsp70 and TSG101 in the extracted precipitates but negative expression of Calnexin (Fig. 1F). Subsequently, we detected the levels of miR-29b-3p in Exos-29b-ago and Exos-29b-anta. The results showed that the expression level of miR-29b-3p in the control exosomes (Exos-NC) was limited, which increased significantly (158963 times higher, $P < 0.01$) or decreased in the Exos-29b-ago and Exos-29b-anta, respectively (Fig. 1G). In summary, we successfully constructed exosomes carrying miR-29b-3p (Exos-29b-ago), exosomes silence miR-29b-3p (Exos-29b-anta).

Exosome Tracking on Injured Corneas and iHCECs

To explore whether carrying miR-29b-3p influences the uptake of exosomes by corneal tissue and cells, we used Dil to label Exos-29b-ago and Exos-NC to perform an Exos tracing investigation in both vivo and vitro. The unlabeled Exos-NC was set as control (Ctrl). The results of confocal laser scanning microscopy of corneal-stretched preparations showed that after 24 hours of topical application of Exos, many Dil-labeled Exos were visible, especially in the wound gap on the corneal surface, and infiltrated into the deep layer of the cornea (Fig. 1H).

Exos-29b-ago Alleviated the Corneal Inflammatory and Corneal Haze in CI Mice

After establishing the CI model, we treated CI mice according to the grouping. Three days (day 3) after treatment, the slit-lamp results showed that in the injury control group (PBS), there was significant central and peripheral corneal edema without visible pupils, obvious ciliary hyperemia, and neovascularization (Fig. 2A). The H&E results showed that in the PBS group, there were one to two layers of epithelial cell migration at the edge of the corneal wound and more inflammatory cell infiltration was observed at the edge of the wound. Corneal stromal collagen fiber lamellae were swollen and corneal thickness was increased (Fig. 2B). These results indicated a severe inflammatory response in the PBS group. Treatment by different Exos alleviated the corneal inflammatory and corneal haze to different extents. Among them, Exos-29b-ago and Exos-29b-anta showed the best and the worst anti-inflammatory effects, respectively. The Exos-29b-ago group mice had only mild corneal edema, visible iris details and pupils, and mild ciliary congestion (see Fig. 2A). There was no significant difference in epithelial healing between the Exos-29b-ago and the Exos-NC groups. The H&E results showed that in the Exos-29b-ago group, 1 to 2 layers of epithelial cell migration were observed at the wound edge, and only a small amount of inflammatory cell infiltration was observed in the stroma layer (see Fig. 2B). The results of the clinical inflammatory index at day 3 showed that it was of the PBS group (0.85 ± 0.10) and was significantly higher than that of the treatment group (from low to high): Exos-29b-ago (0.22 ± 0.08, $P < 0.01$), Exos-NC (0.53 ± 0.12, $P < 0.01$), and Exos-29b-anta (0.77 ± 0.12). The Exo-29b-ago group showed the lowest index among all groups (Fig. 2C).

Seven days after treatment (day 7), the slit-lamp results showed that corneal edema, opacity with iris details invisible, and corneal neovascularization were observed in the PBS group (see Fig. 2A). The H&E staining results showed that in the PBS group, the corneal stroma swelled, keratocytes proliferated in the superficial lamellae, inflammatory cells infiltrated, and corneal thickness was increased, indicat-

Investigative Ophthalmology & Visual Science

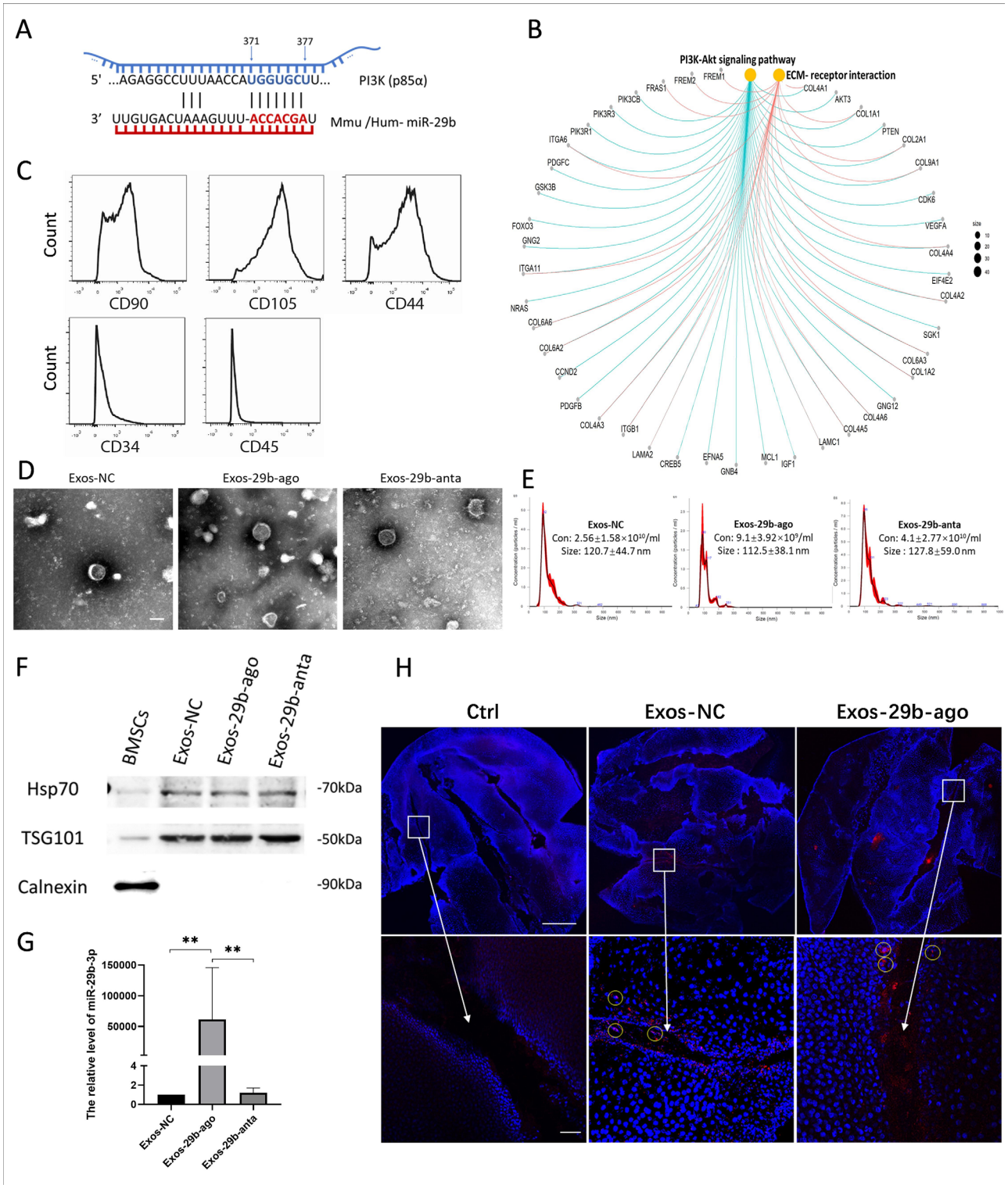

Figure 1. Characterizations of BMSCs and BMSC-Exos. (**A**) TargetScan and miRDB showed PI3K(p85a) was a direct target of miR-29b-3p. (**B**) KEGG pathway enrichment analysis showed miR-29b-3p might related to the PI3K/AKT pathway. (**C**) Flow cytometry results for the expression of BMSCs markers: CD90, CD105, CD44, CD34, and CD45. (**D**) TEM images of Exos-NC, Exos-29b-ago, and Exos-29b-anta. Scale bar = 100 nm. (**E**) NTA results of size distribution of Exos-NC, Exos-29b-ago and Exos-29b-anta. Con means concentration. (**F**). Western blot showed the expression of the markers: HSP70, TSG101, and Calnexin of Exos-NC, Exos-29b-ago, and Exos-29b-anta. The protein of BMSCs served as the control group. (**G**) RT-qPCR showed the levels of miR-29b-3p of Exos-NC, Exos-29b-ago, and Exos-29b-anta ($n = 3$). $^{**}P < 0.01$. (**H**) Dill-labeled (*red*) Exos-NC and Exos-29b-ago tracking. DAPI (*blue*) show the surface of the corneal stretched preparation. Exos-NC without Dil-label set as the Ctrl. The *circle* indicated the cells in the cornea stained with Dil-labeled Exos. Scale bar = 1000 and 50 µm.

Investigative Ophthalmology & Visual Science

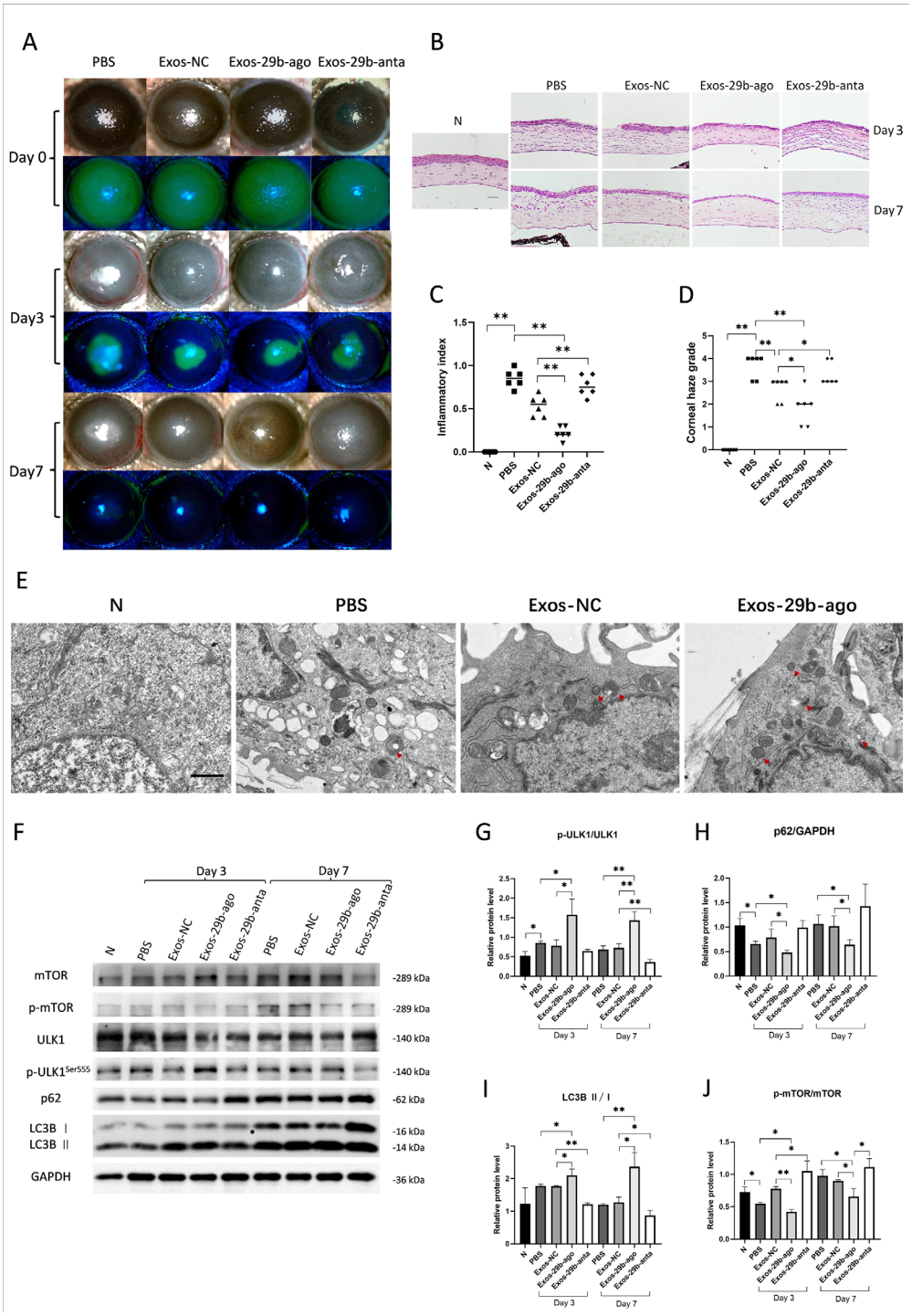

Figure 2. Exos-29b-ago alleviated the corneal inflammatory, corneal haze, and activated autophagy in the cornea of CI mice. (**A**) Cornea fluorescein staining photographs and bright field photos of all groups at 3 and 7 days after treatment (day 3 and day 7). (**B**) H&E staining showed the histologic structure of the cornea of all groups. The eyeballs were harvested at day 3 and day 7. Scale bar = 100 µm. (**C**) The corneal inflammatory index of all groups at day 3 ($n = 6$). (**D**) The corneal haze grade of all groups at day 7 ($n = 6$). (**E**) TEM pictures showed there were autophagosomes (double membrane structure, *red arrow*) in the corneal epithelium of CI mice. Scale bar = 1.0 µm. (**F**) The results of expressions of the autophagy marker proteins p-mTOR, mTOR, p-ULK1^{Ser555}, ULK1, p62, LC3BI, LC3BII, and GAPDH in CI mice of all groups at day 3 and day 7. (**G**) Relative expression of the ratios of p-ULK1^{Ser555}/ULK1 ($n = 3$). (**H**) Relative expressions of p62 to GAPDH ($n = 3$). (**I**) Relative expressions of the ratios of LC3BII/I ($n = 3$). (**J**) Relative expression of the ratios of p-mTOR/mTOR ($n = 3$). *$P < 0.05$, **$P < 0.01$.

ing a severe fibrosis response (see Fig. 2B). Similarly, Exos-29b-ago and Exos-29b-anta also showed the best and worst anti-fibrosis effects, respectively. The Exos-29b-ago group showed slight corneal haze with visible irises and pupils and no significant neovascularization (see Fig. 2A). The H&E results showed that the corneal stromal thickness decreased in the Exos-29b-ago group with only a small amount of proliferated keratocytes and inflammatory cells visible. Additionally, among the treatment groups, the collagen fibers in the corneal stroma of the Exos-29b-ago group showed no swelling and were neatly arranged (see Fig. 2B). The results of the corneal haze grade at day 7 showed that it was of the PBS group and was 3.67 ± 0.52, among the exosomes treatment groups, the corneal haze grade of the Exos-29b-3p group (1.67 ± 0.82) was the lowest, the Exos-NC group was 2.83 ± 0.75, and the Exos-29b-anta group was 3.33 ± 0.52 (Fig. 2D). The above results imply that miR-29b-3p is one of the most important components in the BMSCs-Exos. Exos-29b-ago effectively alleviate the corneal inflammatory and fibrosis.

Exos-29b-ago Activated Autophagy in CI Mice

As mentioned above, miR-29b may be involved in the regulation of autophagy which is closely related to cellular and tissue injuries. By removing damaged organelle components, autophagy facilitates the restoration of cellular functions and promotes the repairment of tissue. Therefore, we hypothesize that Exos-29b-ago treatment promotes corneal repairment in CI mice through regulating autophagy. We recorded electron microscopy images to investigate the ultrastructure of the cornea in each group of CI mice. The results showed that compared with the N group, there were more autophagosomes in the corneal epithelial cells of the PBS group, indicating that autophagy was activated in the injured corneal epithelial cells. The number of autophagosomes and autolysosomes in the corneal epithelial cells of the Exos-29b-ago group was significantly increased compared with that of Exos-NC group (Fig. 2E). This result indicated a significant increase in autophagy levels in the corneal epithelium of CI mice after Exos-29b-ago treatment.

We detected autophagy-related proteins in the corneal tissue of each group. ULK1, LC3B, and p62 are recognized as the important proteins which participate in autophagy. ULK1 (is known as Atg1 in yeast) plays a key role perhaps at the most upstream step in the initial stages of autophagy induction.[31] The increased phosphorylation level of ULK1 at the Ser555 site indicates the activation of ULK1 complex, and then activates autophagy.[32] More LC3B conversion (LC3B I to LC3B II) means active autophagosome synthesis.[33] As a bridge between LC3 and polyubiquitinated proteins, p62 is selectively encapsulated in autophagosomes and then degraded by proteolytic enzymes. Therefore, the expression of p62 is negatively correlated with autophagic activity.[34] The Western blot results in this study showed that, on the third day after treatment (day 3), compared with the N group, the expressions of p-ULK1^{Ser555}/ULK1, LC3BII/I in the PBS groups increased, whereas the expression of p62 decreased. Among the Exos treatment groups, the Exo-29b-ago group showed the highest levels of p-ULK1^{Ser555}/ULK1 and LC3BII/I, and the lowest of p62, whereas the Exo-29b-anta group exhibited the lowest levels of p-ULK1^{Ser555}/ULK1 and LC3BII/I, and the highest of p62. On the seventh day after injury (day 7), the expressions of p-ULK1^{Ser555}/ULK1 and LC3B II/I in the PBS groups and other 3 treatment groups decreased compared to those on day 3. However, the expressions of p-ULK1^{Ser555}/ULK1 and LC3B II/I in the Exos-29b-ago group were still the highest among the treatment groups. The expression of p62 in the 4 groups increased compared to that at day 3, whereas the expression of p62 in the Exos-29b-ago group was still the lowest among the 3 groups (Figs. 2F–2I). The above results indicated that in the early stages of injury, autophagy levels in corneal tissues are activated, indicating the activation of basal autophagy. After treatment with Exos-29b-ago, autophagy levels significantly increased in the injured cornea. Additionally, on the seventh day after corneal injury, although autophagy levels decreased in injury control group (PBS), they remained elevated in the corneas of the Exos-29b-ago treatment group.

mTOR is an important regulatory protein in autophagy. mTOR is activated typically under nutrient-rich conditions and directly inhibits the initiation of autophagy by preventing ULK1 from interacting with other autophagy-initiating proteins.[35] Therefore, we detected the levels of mTOR activation in the cornea of CI mice. The Western blot results indicated that among the treatment groups, the Exo-29b-ago group showed the lowest level of p-mTOR/mTOR, whereas the Exo-29b-anta group exhibited the highest level of p-mTOR/mTOR (see Figs. 2F, 2J). It consisted with the results of the expression of p-ULK1^{Ser555}/ULK1, LC3BII/I, and p62.

In summary, autophagy levels in corneal tissues are activated at the early stage after corneal injury, but subsequently decrease. Exos-29b-ago can enhance autophagy, thereby ameliorating inflammatory and fibrosis following corneal injury. Conversely, the therapeutic effects of exosomes inhibiting miR-29b-3p (Exos-29b-anta) are significantly diminished. It suggests that Exos-29b-ago might be a promising therapeutic approach for promoting repairment of corneal injury. Consequently, detailed validation was conducted on the mechanism of Exos-29b-ago to promoting the repair of corneal injury in the follow-up studies.

Anti-Inflammatory Effect of Exos-29b-ago by Inhibiting the PI3K/AKT/mTOR/NF-κB Pathway in CI Mice

Based on the previous researches mentioned above and the results of this study, we hypothesized that miR-29b-3p regulates autophagy through inhibition of the PI3K/AKT/mTOR signaling pathway.

The levels of miR-29b-3p in the corneal tissue of CI mice in each group was detected. Three days after treatment, the levels of miR-29b-3p in the corneas of Exos-29b-ago group were 6.01 times higher than those in the PBS group ($P < 0.01$), and were 2.71 times higher than in the Exos-NC group ($P < 0.05$). Seven days after treatment, the miR-29b-3p levels in the Exos-29b-ago group were 8.74 times than those of the PBS group ($P < 0.01$), and were 3.11 times those of the Exos-NC group ($P < 0.05$; Fig. 3A).

The Western blot results showed that at day 3 after injury, compared with the N group, the phosphorylation level of PI3K (p-PI3K/PI3K) increased in the PBS group ($P < 0.01$). In addition, after Exos-29b-ago treatment, as the target gene of miR-29b-3p, PI3K (p85α) was significantly reduced compared with that in the Exos-NC groups ($P < 0.01$), along with a decrease in the level of p-PI3K/PI3K and p-AKT/AKT. At day 7 after treatment, the expressions of

Investigative Ophthalmology & Visual Science

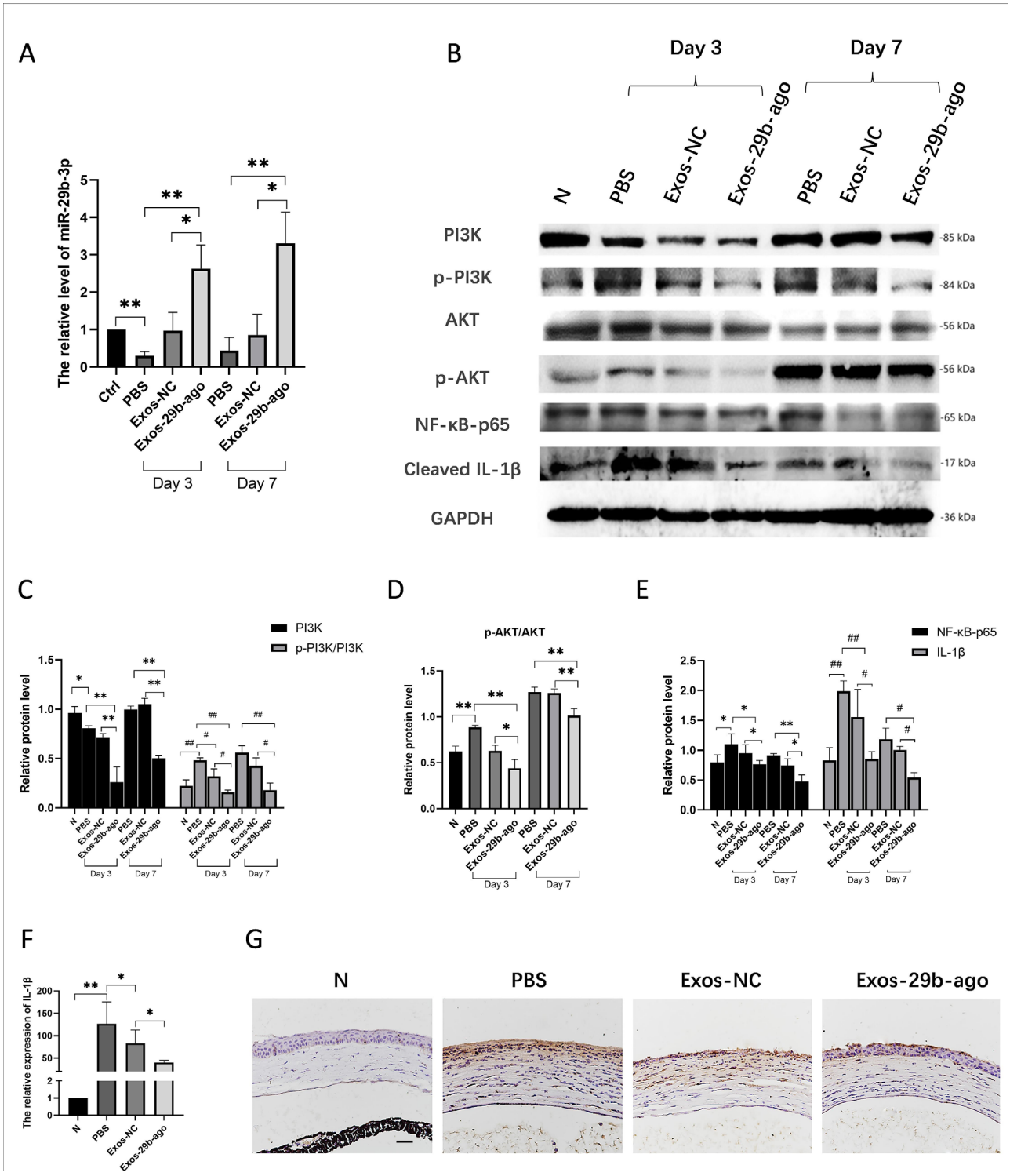

Figure 3. Exos-29b-ago inhibited the PI3K/AKT signaling and NF-κB/IL-1β signaling in CI mice. (**A**) RT-qPCR showed the levels of miR-29b-3p of cornea tissue of all groups at day 3 and day 7 ($n = 3$). (**B**) The Western blot results of proteins of PI3K/AKT and NF-κB/IL-1β signaling pathway in CI mice of all groups. (**C**) Relative expression of PI3K to GAPDH and the ratios of p-PI3K/PI3K in CI mice of all groups ($n = 3$). (**D**) The ratio of p-AKT/AKT in CI mice of all groups ($n = 3$). (**E**). Relative expression of NF-κB-p65, cleaved IL-1β to GAPDH ($n = 3$). (**F**). RT-qPCR showed the expression of IL-1β in cornea of CI mice ($n = 3$). (**G**) Immunohistochemical analysis of IL-1β expression, Scale bar = 100 µm.

PI3K, p-PI3K/PI3K, and p-AKT/AKT in all groups increased compared with those at day 3. The Exos-29b-ago still had the lowest level of PI3K, p-PI3K/PI3K, and p-AKT/AKT among them (Figs. 3B–3D). The results showed that after Exos-29b-ago treatment, PI3K/AKT signaling pathway was significantly inhibited. The above results are consistent with the autophagy-related protein results.

According to previous research, autophagy is closely related to inflammation.[4,6] Through slit-lamp and H&E staining analyses, we found that after Exos-29b-ago treatment, inflammation in the CI corneas significantly reduced. Therefore, we detected the expressions of NF-κB-p65 and cleaved IL-1β through Western blot. The results showed that (see Figs. 3B, 3E), in the early stages of repair (day 3), in the Exos-29b-ago group, the expressions of NF-κB-p65 and cleaved IL-1β both significantly decreased compared to those in the Exos-NC group ($P < 0.05$ and $P < 0.05$). The results of RT–qPCR (Fig. 3F) and immunohistochemistry (Fig. 3G) at day 3 after treatment also indicated that the expression of cleaved IL-1β decreased in the Exos-29b-ago group. The Western blot results of day 7 after treatment also confirmed the above results.

In summary, after Exos-29b-ago treatment, the PI3K/AKT/mTOR pathway in the corneal tissue of CI mice was inhibited, thereby activating autophagy and inhibiting inflammation.

Anti-Fibrosis Effect of Exos-29b-ago by Inhibiting the Fibrosis-Related Genes in CI Mice

We evaluated corneal fibrosis at the later stage of corneal wound healing in CI mice. The results of slit lamp showed that after 7 days (day 7) of treatment, the corneal epithelium in all groups had healed. At day 14 after treatment, corneal edema was reduced by various extents in all groups. Corneal pannus formed on the surface of the cornea in the PBS group. In the Exos-29b-ago group, only mild corneal haze was observed, with visible irises and pupils (Fig. 4A). Additionally, after corneal opacity quantitative analysis, the results showed that the corneal haze grade of the Exos-29b-ago group (1.33 ± 0.52) was significantly decreased compared with that of the Exos-NC group (2.17 ± 0.75, $P < 0.05$), respectively ($n = 6$; Fig. 4B). The H&E staining results are consistent with the above findings. The corneal morphology of the Exos-29b-ago group is most similar to that of the N group (Fig. 4E).

The RT–qPCR results showed that, at day 14 after treatment, the level of miR-29b-3p in the Exos-29b-ago group was 12.5-fold that in the PBS group ($P < 0.05$) and 4.96-fold that in the Exos-NC group ($P < 0.05$; Fig. 4C). To further explore the antifibrotic mechanism of Exos-29b-ago in CI mice, we detected the expression of genes related to fibrosis, such as collagen type III alpha 1 chain (COLIII), α-SMA, fibronectin 1 (FN), and vimentin (Vim), in all groups at day 7 and day 14 after Exos treatment. The results of RT–qPCR (Fig. 4D), immunofluorescence (Figs. 5A, 5C, 5D) and immunohistochemistry (Fig. 5B) showed that the above genes were significantly upregulated in the PBS group at day 7 and day 14 compared to the N group. The above genes in the Exos-29b-ago group were significantly reduced compared to those in the Exos-NC groups. In summary, Exos-29b-ago can effectively promote corneal stroma repair and inhibit corneal opacity in CI mice through inhibiting the expressions of fibrosis-related genes.

Effects of miR-29b-3p on the Regulation of Autophagy in iHCECs by Inhibiting PI3K/AKT/mTOR/NF-κB Signal Transduction in iHCECs

Previous researches confirmed that the LPS induces a significantly decreased expression of miR-29b in various cells.[36–38] For instance, study showed that compared to healthy individuals, miR-29b expression was reduced in the plasma of sepsis patients. LPS induced decrease expression of miR-29b in cardiomyocytes, and overexpression of miR-29b significantly alleviated the inflammatory in cardiomyocytes.[39] Other research demonstrated that radiation exposure causes a downregulation of miR-29b in blood vessels, thereby promoting an inflammatory, whereas overexpression of miR-29b can effectively suppress vascular inflammation.[40] Consequently, we investigated the expression of miR-29b-3p and the autophagy level in iHCECs induced by LPS.

The iHCECs were treated by 200 ng/mL of LPS to investigate to the correlation between the expression of miR-29b-3p and the level of autophagy. The treatment times were set at a gradient of 3, 6, 12, 24, and 48 hours to observe the dynamics expression of miR-29b-3p over time. The results of RT-qPCR demonstrated that the expression of miR-29b-3p was significantly downregulated at 6 hours post-treatment ($P < 0.01$), showing a continued decrease thereafter (Fig. 6A). Subsequently, we detected the expression of autophagy-related proteins in iHCECs treated with LPS. The results showed that in the early stages of LPS treatment (3 hours and 6 hours), the autophagy of iHCECs was activated, as the expression of p-ULK1^{Ser555}/ULK1 and LC3II/I were increased. With extended exposure to LPS in iHCECs (12-48 hours), the level of autophagy in iHCECs gradually decreases, as the expression of p-ULK1^{Ser555}/ULK1 and LC3II/I were decreased, accompanied by the increased expression of p62 (Figs. 6B, 6C). The above results indicate that a decreased level of miR-29b-3p is associated with reduced autophagy. These results implied the potential regulatory correlation between miR-29b-3p and autophagy in iHCECs.

Consequently, iHCECs transfected were treated with 200 ng/mL of LPS for 24 hours. The RT–qPCR results showed that after LPS treatment, the expression of miR-29b-3p was downregulated in the iHCECs compared to that in the Ctrl group ($P < 0.05$). Compared with that in the ago NC+LPS group, the level of miR-29b-3p in the ago miR-29b+LPS group increased ($P < 0.05$). The level of miR-29b-3p in the anta miR-29b+LPS group decreased compared to that in the anta NC + LPS group ($P < 0.05$; Fig. 6D). These results indicated that the miR-29b-3p agomir was successfully transfected into the iHCECs. The Western blot results showed that, compared with the Ctrl group, the LPS group showed a significantly decreased expression of p-ULK1^{Ser555}/ULK1 and LC3B II/I in iHCECs, accompanied by significantly increased expression of p62. The expression of p-ULK1^{Ser555}/ULK1 and LC3B II/I was upregulated in the ago miR-29b+LPS group, accompanied by downregulation of p62 expression compared with that in the ago NC+LPS group. The expression of p-ULK1^{Ser555}/ULK1 and LC3B II/I in the anta miR-29b+LPS group was downregulated and accompanied by upregulation of p62 expression compared with that in the anta NC + LPS group (Figs. 6E, 6F). The results showed that after overexpression of miR-29b-3p, autophagy in the

Investigative Ophthalmology & Visual Science

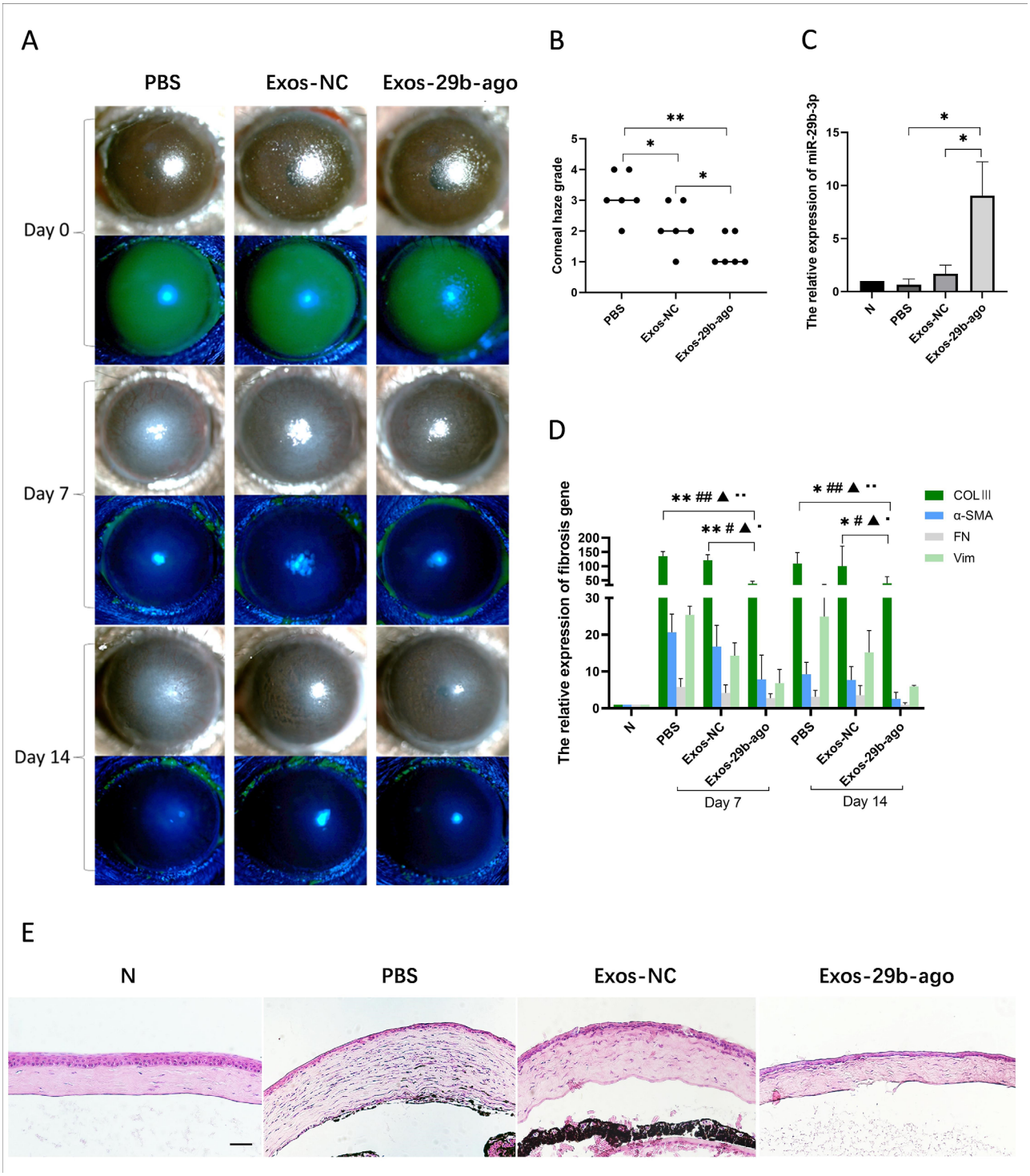

Figure 4. Exos-29b-ago inhibited the fibrosis-related genes in CI mice. (**A**) Cornea fluorescein staining photographs and bright field photographs of all groups at 7 days and 14 days after treatment (day 7 and day 14). (**B**) The corneal haze grade of all groups at day 14 ($n = 6$). *$P < 0.05$, **$P < 0.01$. (**C**). RT-qPCR showed the levels of miR-29b-3p of cornea tissue of all groups at day 14 ($n = 3$). *$P < 0.05$. (**D**) RT-qPCR showed the expression of COLIII, α-SMA, FN, and Vim of cornea tissue of all groups at day 7 and day 14 ($n = 3$). * for COLIII, # for α-SMA, ▲ for FN1, and ● for Vim. *, #, ▲, and ● $P < 0.05$; **, ##, ▲▲, and ●● $P < 0.01$. (**E**) H&E staining showed the histologic structure of cornea of all groups. The eyeballs were harvested at day 14. Scale bar = 100 µm.

iHCECs was significantly activated. Subsequently, the regulatory effect of miR-29b-3p on the PI3K/AKT/mTOR pathway was also verified. The Western blot results showed that in comparison to the Ctrl group, the expressions of p-PI3K/PI3K, p-AKT/AKT, and p-mTOR/mTOR in the iHCECs of the LPS group were elevated. Compared with the ago NC+LPS groups, the expression levels of p-PI3K/PI3K, p-AKT/AKT, and p-mTOR/mTOR in the ago miR-29b+LPS

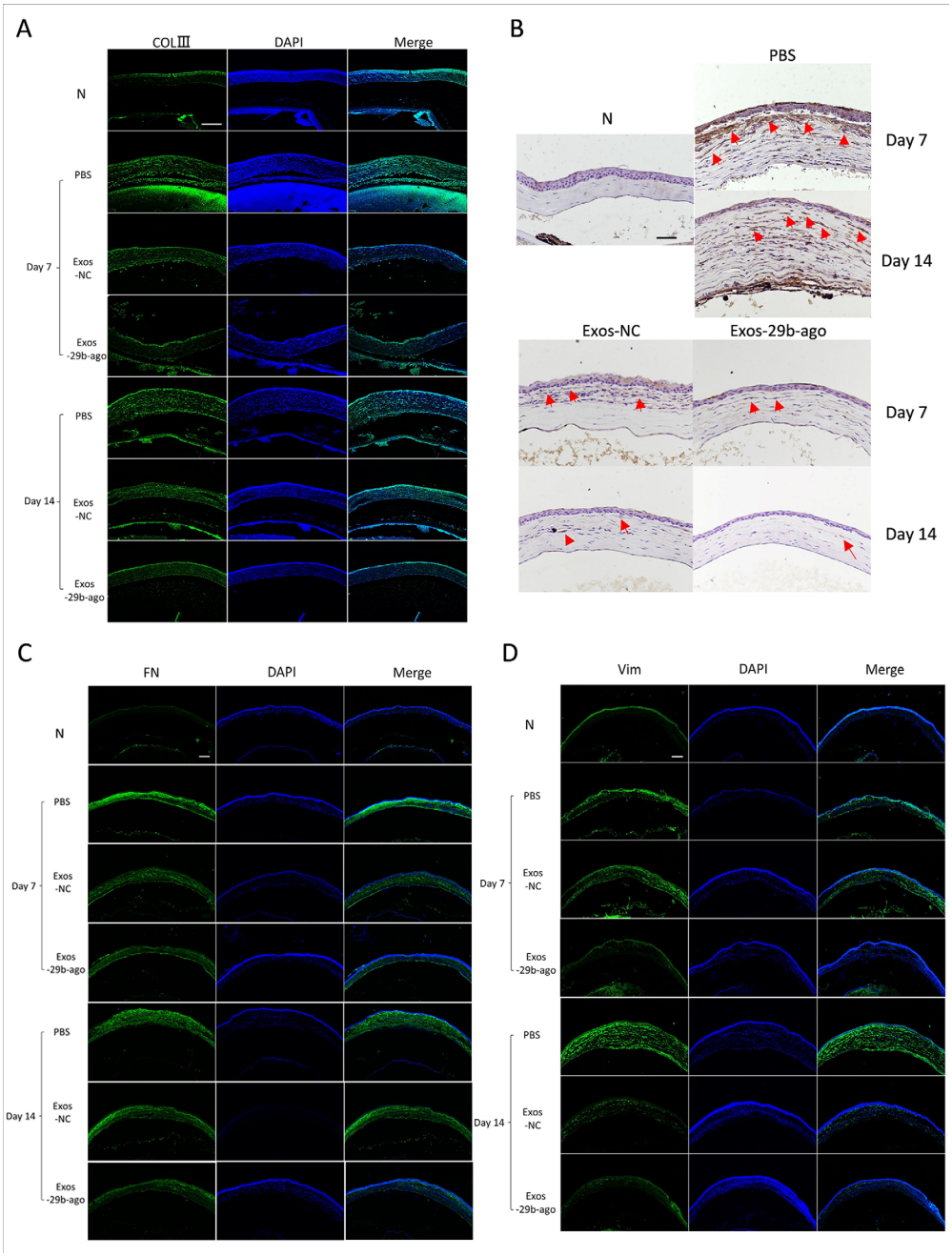

Figure 5. Immunofluorescence and immunohistochemical results of the fibrosis-related genes in CI mice. (**A**) Immunofluorescence analysis of COLIII expression. Scale bar = 200 µm. (**B**) Immunohistochemical analysis of α-SMA expression. Scale bar = 100 µm. (**C**) Immunofluorescence analysis of FN expression. Scale bar = 200 µm. (**D**) Immunofluorescence analysis of Vim expression. Scale bar = 200 µm.

group significantly decreased. Compared to those in the anta NC+LPS group, the expressions of p-PI3K/PI3K, p-AKT/AKT, and p-mTOR/mTOR in the anta miR-29b+LPS group were upregulated (Figs. 6G-6J). The above results indicated that LPS stimulation can activate the PI3K/AKT/mTOR pathway, whereas overexpression of miR-29b-3p inhibits the PI3K/AKT/mTOR pathway.

In addition, we detected the expression of NF-κB-p65 and cleaved IL-1β in each group. The expressions of NF-κB-p65 and cleaved IL-1β in the iHCECs of the LPS group were significantly increased compared to that in the iHCECs of the Ctrl group, as shown by Western blot. Compared with the ago NC+LPS groups, the expression levels of both NF- κB-p65 and IL-1β significantly decreased in the ago miR-29b+LPS group. In contrast, the above results were also verified in the anta miR-29b+LPS group. Compared to those in the anta NC+LPS group, the expressions of NF-κB-p65 and IL-1β in the anta miR-29b+LPS group were upregulated (Figs. 6G, 6K). We also tested the mRNA expression of IL-1β in each group of iHCECs (Fig. 6L) and the content of IL-1β in the supernatant of the iHCEC cell culture medium in each group

Investigative Ophthalmology & Visual Science

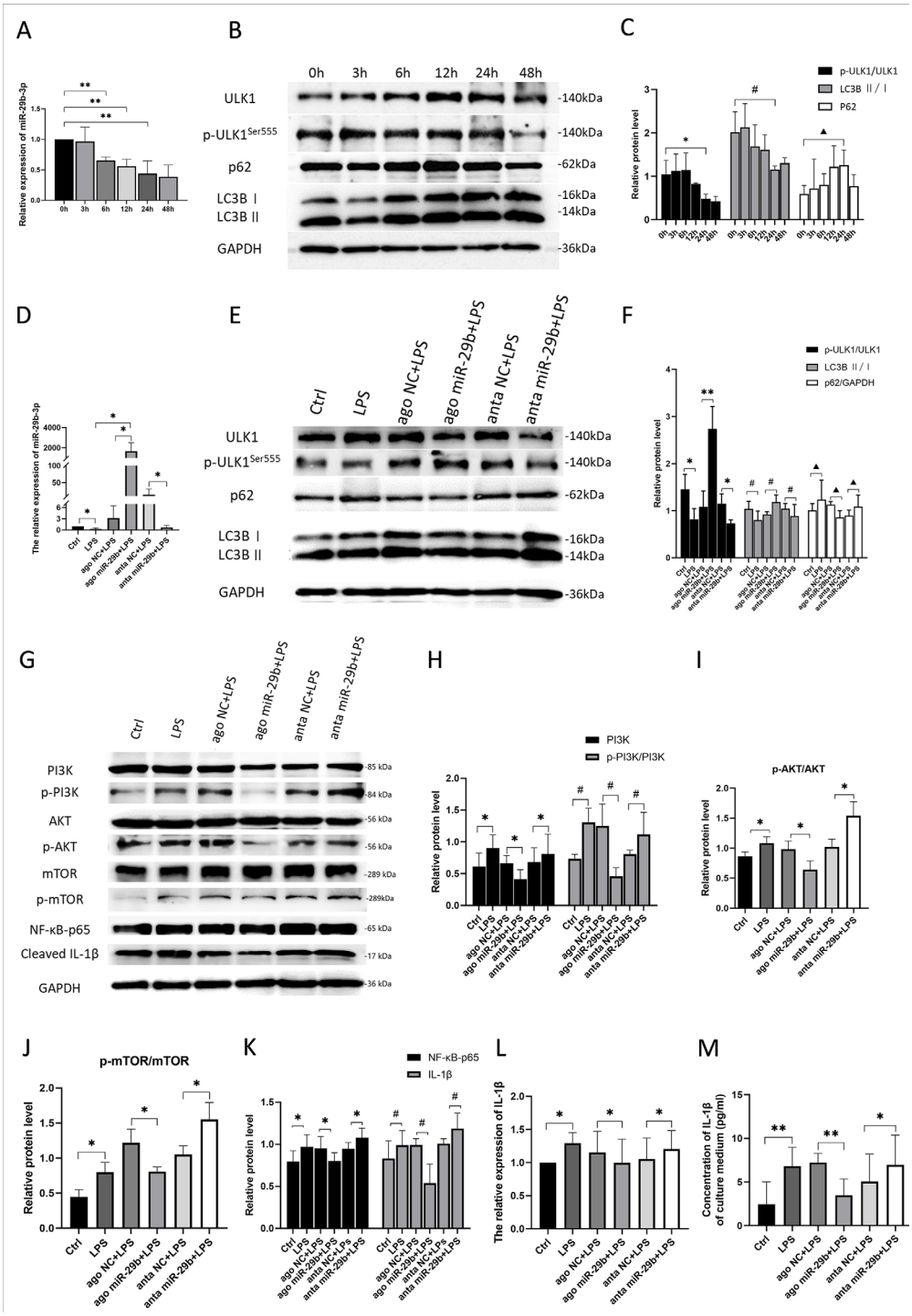

Figure 6. MiR-29b-3p activated autophagy and suppressed inflammation via inhibiting PI3K/AKT/mTOR signaling pathway on iHCECs. (**A**) The results of RT-qPCR showed the levels of miR-29b-3p in iHCECs treated with 200 ng/mL LPS after 3 hours, 6 hours, 12 hours, 24 hours, and 48 hours ($n = 3$). (**B**) The Western blot results of levels of the autophagy marker proteins p-ULK1^{Ser555}, ULK1, p62, LC3BI, LC3BII, and GAPDH in iHCECs treated with 200 ng/mL LPS after 3 hours, 6 hours, 12 hours, 24 hours, and 48 hours. (**C**) Relative expressions of the ratios of p-ULK1^{Ser555}/ULK1, p62 to GAPDH and the ratios of LC3BII/I ($n = 3$). (**D**) The results of RT-qPCR showed the levels of miR-29b-3p in iHCECs transfected with miR-29b-3p agomir/antagomir and then treated with 200 ng/mL LPS (24 hours, $n = 3$). (**E**) The Western blot results of levels of the autophagy marker proteins p-ULK1^{Ser555}, ULK1, p62, LC3BI, LC3BII, and GAPDH in iHCECs transfected with miR-29b-3p agomir/antagomir and then treated with 200 ng/mL LPS (24 hours). (**F**) Relative expression of the ratios of p-ULK1^{Ser555}/ULK1, p62 to GAPDH, and LC3BII/I ($n = 3$). (**G**) The Western blot results of the levels of the autophagy marker proteins, p-PI3K, PI3K, p-AKT, AKT, p-mTOR, and mTOR, and inflammatory related proteins, NF-κB-p65, and cleaved IL-1β, in iHCECs transfected with miR-29b-3p agomir/antagomir and then treated with 200 ng/mL LPS (24 hours). (**H**) Relative expression of PI3K to GAPDH and the ratios of p-PI3K/PI3K on iHCECs ($n = 3$). (**I**) The ratios of p-AKT/AKT on iHCECs ($n = 3$). (**J**) The ratios of p-mTOR/mTOR on iHCECs ($n = 3$). (**K**) Relative expression of NF-κB, cleaved IL-1β to GAPDH on iHCECs ($n = 3$). (**L**) RT-qPCR showed the expression of IL-1β in iHCECs ($n = 3$). (**M**) The concentration of IL-1β in the culture medium of iHCECs (pg/mL) ($n = 3$) *, #, ▲$P < 0.05$; **, ##, ▲▲ $P < 0.01$.

Investigative Ophthalmology & Visual Science

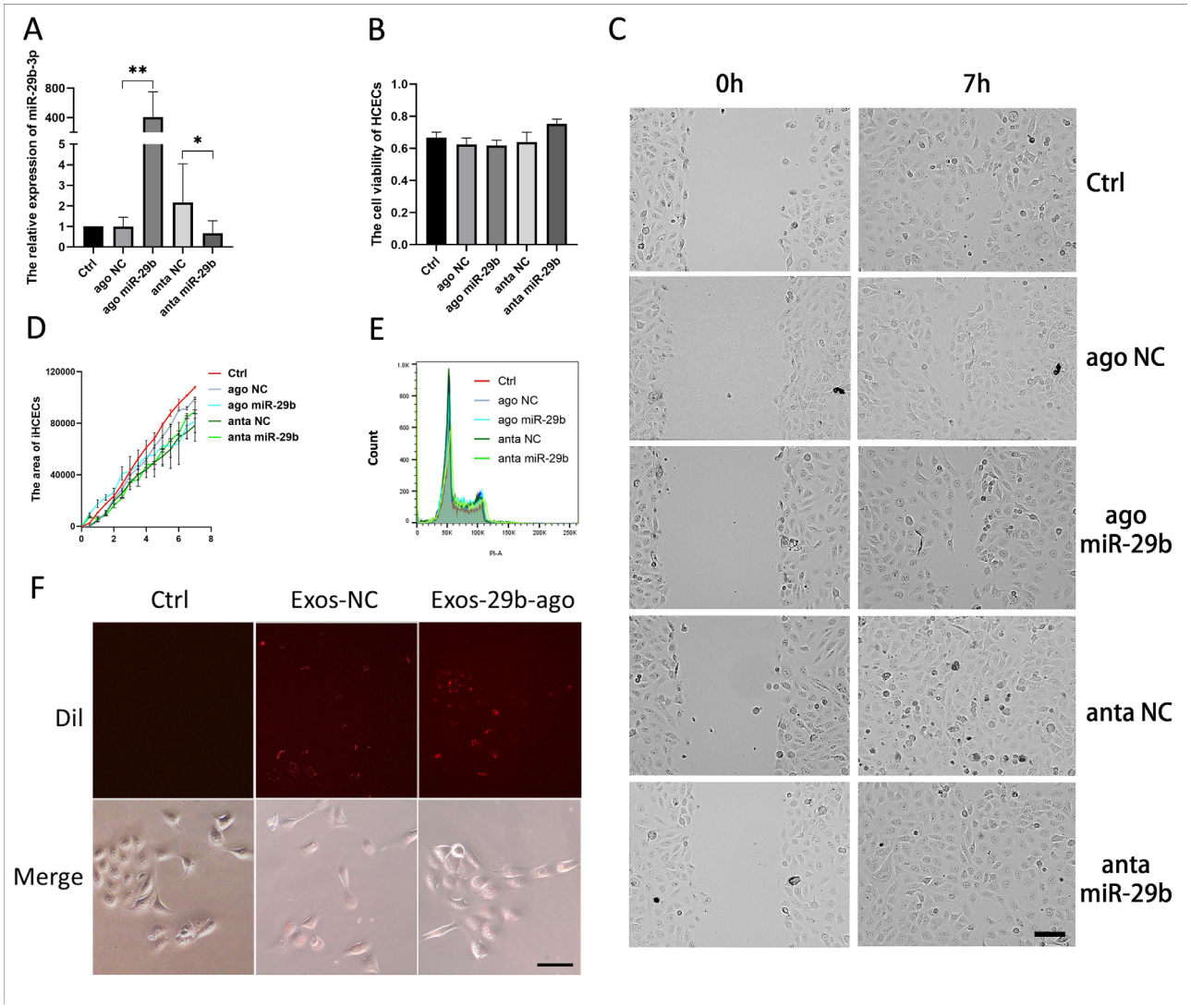

Figure 7. Effects of miR-29b-3p in cell migration, cell proliferation and cell viability on iHCECs in vitro. (**A**) The results of RT-qPCR showed the levels of miR-29b-3p in iHCECs after transfection ($n = 3$). (**B**) The CCK-8 assay for cell viability of iHCECs after transfection ($n = 3$). *$P < 0.05$; **$P < 0.01$. (**C**) The results of wound healing in iHCECs showed the condition of gap at 0 hour and 7 hours, Scale bar = 50 µm. (**D**) The area of iHCECs within the gap (Sum Area $_{\text{time point}}$- Sum Area $_{0\ \text{hour}}$) of iHCECs ($n = 3$). (**E**) The results of flow cytometry for cell cycle composition of iHCECs after transfection ($n = 3$). (**F**) Dil-labeled (*red*) Exos-NC and Exos-29b-ago tracking in the iHCECs. Exos-NC without Dil-label set as Ctrl. The iHCECs incubated with Dil-labeled Exos for 12 hours (20 ×).

(Fig. 6M). The results are consistent with the Western blot results.

In summary, miR-29b-3p activates autophagy in iHCECs and suppresses inflammatory by inhibiting the PI3K/AKT/mTOR pathway.

Effects of miR- 29b-3p on the Viability, Proliferation, and Migration of iHCECs

The results of previous studies showed that miR-29b has a certain impact on the cell cycle, cell proliferation, and cell migration of various tumor cells.[41] Therefore, we verified whether miR-29b-3p has an impact on the viability, proliferation, and migration of iHCECs. First, we transfected iHCECs with miR-29b-3p agomir (Ago miR-29b) and its control (ago NC), miR-29b antagomir (anta miR-29b) and its control (anta NC), and the transfection reagent only (Ctrl). The RT–qPCR results indicated that the miR-29b agomir was successfully transfected into iHCECs (Fig. 7A). The CCK-8 results showed no difference in cell viability regardless of whether miR-29b-3p was overexpressed (Fig. 7B). The wound healing experiment showed that when miR-29b-3p was overexpressed, there was no significant difference in cell migration ability between the groups (Figs. 7C, 7D). The results of flow cytometry showed that there was no difference in the cell proliferation cycle of all groups (Fig. 7E). We added Dil-labeled Exos-29b-ago and Exos-NC to iHCEC culture medium. After 12 hours, we observed the cells and found that Dil-labeled Exos were visible in both groups of iHCECs, and there was no difference between the two groups (Fig. 7F). The above results indicated that carrying miR-29b-3p does not affect the uptake of exosomes by iHCECs.

In summary, overexpression of miR-29b-3p did not significantly affect cell viability, proliferation, or migration in the normal iHCECs.

Discussion

Autophagy is a self-healing mechanism of cells in response to stress and injury, so the level of autophagy tends to increase in the early stages of injury. Previous studies confirmed that core autophagy machinery exists in platelets. At the early stage of wound healing, autophagy is activated in platelet via LC3 turnover and is essential for platelet function.[42] This study also confirmed that in the mouse model of spinal cord injury, the expressions of Becline 1 and LC3II/I increased at the early stage after injury (on 1–3 days after injury), which implied that the level of autophagy in spinal cord tissue increased. However, on the seventh day after injury, the expressions of Becline 1 and LC3II/I were decreased than those at day 1 and day 3.[43] These are consistent with the results of our findings. The results of this study indicated that the expressions of p-ULK1Ser555/ULK1 and LC3II/I in the PBS group were higher than those in the N group at 3 days after corneal injury, accompanied by a downregulation of p62 expression. This confirms that injury disrupts autophagy homeostasis, leading to the activation of basal autophagy in corneal tissue. Following 7 days of corneal injury, autophagy levels in corneal tissue decrease. Treatment with Exos-29b-ago significantly increases autophagy levels in corneal tissue on both day 3 and day 7 after injury, reducing corneal inflammation and fibrosis.

The miRNAs are endogenous non-coding RNAs and are approximately 22 nt. The miRNAs play negative regulatory roles to their target mRNAs via cleavage or translational repression. The miRNAs comprise one of the more abundant classes of gene regulatory molecules in multicellular organisms.[44] A number of studies have found that repressed levels of miR-29 family (contains 3 members including miR-29a, miR-29b, and miR-29c) have been linked to several fibrosis-related responses and diseases.[45,46] In addition, as mentioned above, it has been confirmed via sequencing that the level of miRNA-29b decreased in various fibrosis and inflammation disease. Among the complications of corneal injuries and keratitis, corneal fibrosis and inflammation could lead to severe visual impairment. That is why miRNA-29b primarily draws our attention. In addition, many studies have found that miR-29b exist in some types of Exos (exosomal miR-29b) and the treatment effect relies on it. For example, exosomal miR-29b originating from pancreatic cancer cells protected human umbilical vein endothelial cells from angiogenesis.[47] This study also confirmed that ultraviolet radiation B irradiation inhibited miR-29b-3p levels compared with controls, but exosomal miR-29b derived from BMSCs treatment restored miR-29b-3p levels and repaired oxidative stress.[48] That also could explain that, in our study compared to the PBS, the Exos-NC also had slightly therapeutic effect. We transfected miR-29b-3p agomir into BMSCs and collected the Exos which accumulated a large amount of miR-29b-3p. It could make miR-29b-3p exert better on ameliorating corneal inflammation and fibrosis.

In recent years, studies have shown that, along with directly targeting fibrosis-related genes, miR-29b can also inhibit various signaling pathway, such as the PI3K/AKT pathway,[16,49] TGF-β/Smad3 pathway,[13] and Wnt pathway.[50] Among them, PI3K/AKT pathway and its relationship with autophagy were eye-catching. Because, on the one hand, research has confirmed that there is a causal relationship between some inflammatory (another key factor in the process of cornea wound healing) and autophagy.[51] The autophagy has been confirmed that it inhibited the aggregation of inflammatory vesicles and degrade IL-1 via DNA degradation, reactive oxygen species degradation, and inhibition of the precursor of IL-1β.[52] Our study also backs these up. We found that PI3K (p85α) was a target gene of miR-29b-3p, and overexpression of miR-29b-3p suppresses the PI3K/AKT/mTOR pathway, further inhibiting the expressions of NF-κB and IL-1β.

As mentioned above, previous researches confirmed that the LPS induces a significantly increased inflammatory responses and decreased expression of miR-29b in various cells. Therefore, in order to explore the correlation between miR-29b-3p and autophagy, we treated iHCECs with LPS in this study. The results indicated a significant decrease in the expression of miR-29b-3p in iHCECs after LPS treatment. The Western blot results showed that in the early stages of LPS treatment, the autophagy of iHCECs was activated, whereas with the prolongation of LPS stimulation time, the level of autophagy in iHCECs gradually decreases accompanied by the decreased miR-29b-3p expression. Although LPS and TNF have been confirmed to induce autophagy in macrophages and other cells.[53,54] Currently, there are still few studies on the regulation of autophagy level in corneal epithelial cells treated by LPS. With the development of research, many studies confirm that LPS induce autophagy impairment in various cells including both immune and non-immune cells. Research demonstrated that autophagic flux and expression of Atg genes in microglia were significantly suppressed upon toll-like receptors 4 (TLR4) activation by LPS, while autophagy was activated by LPS in macrophages.[55] Other studies have shown that LPS induces autophagy impairment in human intestinal epithelial cells and animal model of colitis via TLR4/MyD88/MAPK signaling pathway, and mTOR inhibitor and autophagy activator significantly inhibited the inflammatory response and oxidative stress injury in experimental colitis.[56] Research has also demonstrated that LPS induces the activation of PI3K/AKT/mTOR signaling pathway in RAW264.7 macrophages, although the autophagy level was not further examined.[57] Overall, the results in this study and the previous researches suggest that at the early stage of LPS treatment, autophagy, as a defense mechanism, clearing oxidative stress products and damaged organelles generated by the inflammatory response to maintain cellular stability and function. Prolonged exposure to LPS may lead to excessive cellular stress responses, which could disrupt the basal function of autophagy. The dynamic changes in the autophagy level may reflect the imbalance between transient adaptation and prolonged stress response in cells. In this study, LPS was used to explore the correlation between the expression of miR-29b-3p and autophagy function. The results showed that the level of miR-29b-3p decreased accompanied with autophagy impairment induced by LPS treatment via activation of the PI3K/AKT/mTOR signaling pathway. Upregulation of miR-29b-3p plays a role in activation of autophagy and inhibition of inflammation in iHCECs. However, the mechanism of LPS on autophagy regulation still needs to be confirmed and discussed by a large number of studies and will become one of the future research directions for us. It not only contributes to understanding the role of autophagy in repairment of corneal injury but also has substantial implications for the development of innovative therapeutic strategies based on the regulation of autophagy.

On the other hand, studies have confirmed that activation of autophagy can inhibit tissue fibrosis. For example,

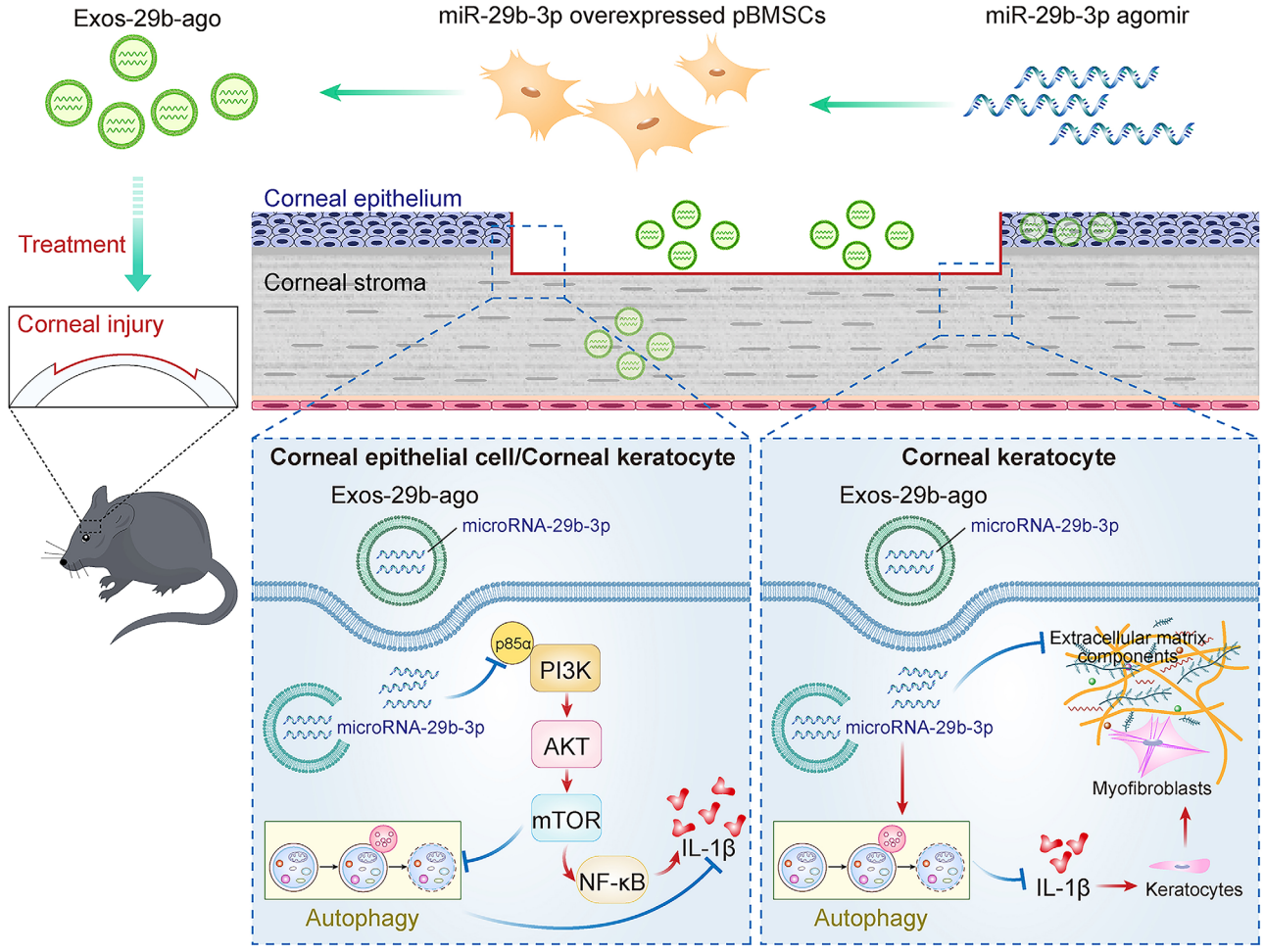

Figure 8. The effect of miR-29b-3p carried by BMSCs-Exos on autophagy activation via inhibiting PI3K/AKT/mTOR pathway and further inhibiting the corneal inflammatory and fibrosis in CI mice.

the results of the study suggested that autophagy in hepatic stellate cells attenuates liver fibrosis by inhibiting the release of fibrogenic extracellular vesicles.[58] In addition, restoring autophagy and suppressing exosome-mediated hepatic stellate cell activation reduces liver fibrosis.[59] The results of our study indicated that overexpression of miR-29b-3p activates autophagy and inhibits the corneal fibrosis-related gene, not only COLIII, but also α-SMA, FN1, and Vim. We considered that it might due to the anti-fibrosis and/or anti-inflammatory effect of autophagy, because the process of traumatic corneal injury healing is a complex interaction between multiple cells. After corneal injury, a large amount of growth factors and cytokines, such as IL-1, are released. IL-1 induces epithelial cells proliferation and migration, and basal stromal keratocyte death, whereas other keratocytes are induced to proliferate and transition from a stationary phenotype to an activated phenotype and further forming fibrosis.[60]

In the present study, the H&E results also suggested obvious inflammatory infiltration at the edge of the corneal epithelium wound accompanied by an increase in IL-1β expression. Meanwhile, we found that the results of H&E and slit lamp showed that the effects of both Exos-29b-ago and Exos-NC to promoting corneal epithelium healing were better than that of the injury control group (the PBS group). In addition, in vitro, overexpression of miR-29b-3p mildly inhibited the cell cycle, cell viability, and cell migration of iHCECs, but the differences were not statistically significant. The result was consistent with previous findings. For example, the results of studies have shown that overexpression of miR-29b-3p may reduce chondrocyte proliferation in osteoarthritis. The miR-29b can inhibit the cell migration of various tumors.[41,61] This is one of the reasons why we chose to use Exos to deliver miR-29b-3p. Utilizing the tissue-repair capacity of Exos to make up for the small deficiency. Significantly, when miR-29b-3p is inhibited (anta miR-29b+LPS group), the expression levels of p62, LC3B I, and LC3B II in iHCECs cells are all upregulated, indicating that the iHCECs will undergo apoptosis or necrosis.[62] The above results indicate that overexpression or inhibition of intracellular miR-29b-3p expression in normal iHCECs does not significantly affect cell viability, cell proliferation, or cell migration. However, when iHCECs are damaged (stimulated by LPS), inhibiting the expression of miR-29b-3p may induce cell apoptosis. Currently, the clinical treatment for corneal fibrosis mainly relies on surgery, such as lamellar keratoplasty and full-thickness penetrating keratoplasty. But due to limited corneal donors, better and more convenient drug treatment has become a focus in this field.

Investigative Ophthalmology & Visual Science

Exosomes, which consist of various components including proteins, mRNAs, miRNAs, and lipids, collectively known as "cargoes," are crucial vesicles for intercellular communication.[63] However, the mechanisms of exosome subcellular processes, including their biogenesis, release, uptake, and the sorting and loading of cargoes, are still largely unknown. Moreover, in research focused on exosomal modification, considerable attention has been paid to the effects of these modifications on the components of exosomes. The cargoes of exosomes determine their functions of signaling transduction, whereas the uptake of exosomes by tissues or cells also affects its functions. In this study, we detected the expression of exosomal marker proteins in all exosomes by Western blot analysis. The results revealed that all exosomal samples exhibited positive expression of Hsp70 and TSG101, accompanied by negative expression of Calnexin, with no significant differences. The morphology, size, and uptake rate of these exosomes in all groups were also similar. Moreover, the uptake of Exos-29b-ago, Exos-29b-anta, and Exos-NC by corneal tissues or iHCECs did not show significant differences. These indicated that exosomes derived from BMSCs were successfully isolated, and overexpression or suppression of miR-29b-3p did not affect the basic structure or fundamental functions of these exosomes. In future research, it will be essential to focus on detailed examinations of alterations in the composition and function of exosomes following genetic modification of cells. This will further facilitate the exploration of the therapeutic potential of exosomes, and enable the development of more effective modifications to improve the therapeutic efficacy of exosomes.

Conclusions

In a CI model, we used exosomes from primary bone marrow mesenchymal stem cells to carry miR-29b-3p for the treatment of injured corneas, further verifying the effects of autophagy activation, inhibition of inflammation, and antifibrosis of cornea by miR-29b-3p. In iHCECs, miR-29b-3p can inhibit the PI3K/AKT/mTOR pathway by targeting PI3K (p85α), further activating autophagy and inhibiting inflammation in iHCECs (Fig. 8).

Acknowledgments

The authors sincerely thank Liu Zuguo (Xiamen University) for providing the iHCECs.

Supported by grants from the National Natural Science Foundation of China (82171024 and 81670837), the Tianjin Science & Technology Foundation (20JCYBJC01450), the Tianjin Health Research Project (TJWJ2023QN080), and the Tianjin Key Medical Discipline (Specialty) Construction Project (TJYXZDXK-016A).

Availability of Data and Materials: The datasets used and/or analyzed during the current study are available from the corresponding author on reasonable request.

Authors' Contributions: Conception and design: J.L., J.G., and X.L. Methodology: J.L., J.G., P.L., Y.W., S.X., R.H., P.H., and X.L. Acquisition of data: J.L. and J.G. Analysis and interpretation of data: J.L., J.G., and Y.Y. Writing, review, and/or revision of the manuscript: J.L., J.G., and X.L. Study supervision: X.L. All authors reviewed the manuscript.

Disclosure: **J. Liu**, None; **J. Gao**, None; **P. Lu**, None; **Y. Wang**, None; **S. Xing**, None; **Y. Yan**, None; **R. Han**, None; **P. Hao**, None; **X. Li**, None

References

1. Mizushima N, Komatsu M. Autophagy: renovation of cells and tissues. *Cell*. 2011;147(4):728–741.
2. Chai P, Ni H, Zhang H, Fan X. The evolving functions of autophagy in ocular health: a double-edged sword. *Int J Biologic Sci*. 2016;12(11):1332–1340.
3. Martin LM, Jeyabalan N, Tripathi R, et al. Autophagy in corneal health and disease: a concise review. *Ocular Surf*. 2019;17(2):186–197.
4. Gao W, Wang X, Zhou Y, Wang X, Yu Y. Autophagy, ferroptosis, pyroptosis, and necroptosis in tumor immunotherapy. *Signal Transduct Target Ther*. 2022;7(1):196.
5. Kim J, Lim YM, Lee MS. The role of autophagy in systemic metabolism and human-type diabetes. *Mol Cells*. 2018;41(1):11–17.
6. Liu B, Deng X, Jiang Q, et al. Scoparone improves hepatic inflammation and autophagy in mice with nonalcoholic steatohepatitis by regulating the ROS/P38/Nrf2 axis and PI3K/AKT/mTOR pathway in macrophages. *Biomed Pharmacother*. 2020;125:109895.
7. Shin CY, Lee S, Jin HL, et al. A small molecule compound that inhibits blue light-induced retinal damage via activation of autophagy. *Biochem Pharmacol*. 2023;211:115534.
8. Tang H, Lin Y, Huang L, Hu J. MiR-223-3p Regulates autophagy and inflammation by targeting ATG16L1 in Fusarium solani-induced keratitis. *Invest Ophthalmol Vis Sci*. 2022;63(1):41.
9. Greene KM, Stamer WD, Liu Y. The role of microRNAs in glaucoma. *Exp Eye Res*. 2022;215:108909.
10. Pu L, Meng Q, Li S, et al. Laminar shear stress alleviates monocyte adhesion and atherosclerosis development via miR-29b-3p/CX3CL1 axis regulation. *J Cell Sci*. 2022;135(14):jcs259696.
11. Han X, Wang S, Yong Z, Zhang X, Wang X. miR-29b ameliorates atrial fibrosis in rats with atrial fibrillation by targeting TGFβRI and inhibiting the activation of Smad-2/3 pathway. *J Bioenerg Biomembr*. 2022;54(2):81–91.
12. Xu Y, Niu Y, Wu B, et al. Extended-release of therapeutic microRNA via a host-guest supramolecular hydrogel to locally alleviate renal interstitial fibrosis. *Biomaterials*. 2021;275:120902.
13. Zhang Y, Huang XR, Wei LH, Chung AC, Yu CM, Lan HY. miR-29b as a therapeutic agent for angiotensin II-induced cardiac fibrosis by targeting TGF-β/Smad3 signaling. *Mol Ther*. 2014;22(5):974–985.
14. Toyono T, Usui T, Villarreal G, Jr., et al. MicroRNA-29b overexpression decreases extracellular matrix mRNA and protein production in human corneal endothelial cells. *Cornea*. 2016;35(11):1466–1470.
15. Liu H, Xiu Y, Zhang Q, Xu Y, Wan Q, Tao L. Silencing microRNA–29b–3p expression protects human trabecular meshwork cells against oxidative injury via upregulation of RNF138 to activate the ERK pathway. *Int J Mol Med*. 2021;47(6):101.
16. Li J, Chan MC, Yu Y, et al. miR-29b contributes to multiple types of muscle atrophy. *Nat Commun*. 2017;8:15201.
17. Xiao X, Li W, Rong D, et al. Human umbilical cord mesenchymal stem cells-derived extracellular vesicles facilitate the repair of spinal cord injury via the miR-29b-3p/PTEN/Akt/mTOR axis. *Cell Death Discov*. 2021;7(1):212.

Investigative Ophthalmology & Visual Science

18. Liang Y, Duan L, Lu J, Xia J. Engineering exosomes for targeted drug delivery. *Theranostics*. 2021;11(7):3183–3195.
19. Batrakova EV, Kim MS. Using exosomes, naturally-equipped nanocarriers, for drug delivery. *J Control Release*. 2015;219:396–405.
20. Lu M, Zhao X, Xing H, et al. Comparison of exosome-mimicking liposomes with conventional liposomes for intracellular delivery of siRNA. *Int J Pharm*. 2018;550(1-2):100–113.
21. Quah BJ, O'Neill HC. The immunogenicity of dendritic cell-derived exosomes. *Blood Cells Mol Dis*. 2005;35(2):94–110.
22. Zheng M, Huang M, Ma X, Chen H, Gao X. Harnessing exosomes for the development of brain drug delivery systems. *Bioconjug Chem*. 2019;30(4):994–1005.
23. Hall J, Prabhakar S, Balaj L, Lai CP, Cerione RA, Breakefield XO. Delivery of therapeutic proteins via extracellular vesicles: review and potential treatments for Parkinson's disease, glioma, and schwannoma. *Cell Mol Neurobiol*. 2016;36(3):417–427.
24. Liu S, Fan M, Xu JX, et al. Exosomes derived from bone-marrow mesenchymal stem cells alleviate cognitive decline in AD-like mice by improving BDNF-related neuropathology. *J Neuroinflammation*. 2022;19(1):35.
25. Mead B, Tomarev S. Bone marrow-derived mesenchymal stem cells-derived exosomes promote survival of retinal ganglion cells through miRNA-dependent mechanisms. *Stem Cells Transl Med*. 2017;6(4):1273–1285.
26. Deng CL, Hu CB, Ling ST, et al. Photoreceptor protection by mesenchymal stem cell transplantation identifies exosomal MiR-21 as a therapeutic for retinal degeneration. *Cell Death Differ*. 2021;28(3):1041–1061.
27. Raposo G, Nijman HW, Stoorvogel W, et al. B lymphocytes secrete antigen-presenting vesicles. *J Exp Med*. 1996;183(3):1161–1172.
28. Movahedan A, Majdi M, Afsharkhamseh N, et al. Notch inhibition during corneal epithelial wound healing promotes migration. *Invest Ophthalmol Vis Sci*. 2012;53(12):7476–7483.
29. Laria C, Alió JL, Ruiz-Moreno JM. Combined non-steroidal therapy in experimental corneal injury. *Ophthalmic Res*. 1997;29(3):145–153.
30. Zhou Y, Wang T, Wang Y, et al. Blockade of extracellular high-mobility group box 1 attenuates inflammation-mediated damage and haze grade in mice with corneal wounds. *Int Immunopharmacol*. 2020;83:106468.
31. Jung CH, Ro SH, Cao J, Otto NM, Kim DH. mTOR regulation of autophagy. *FEBS Lett*. 2010;584(7):1287–1295.
32. Gwinn DM, Shackelford DB, Egan DF, et al. AMPK phosphorylation of raptor mediates a metabolic checkpoint. *Mol Cell*. 2008;30(2):214–226.
33. Mizushima N, Yoshimori T. How to interpret LC3 immunoblotting. *Autophagy*. 2007;3(6):542–545.
34. Ichimura Y, Kumanomidou T, Sou YS, et al. Structural basis for sorting mechanism of p62 in selective autophagy. *J Biol Chem*. 2008;283(33):22847–22857.
35. Yang H, Jiang X, Li B, et al. Mechanisms of mTORC1 activation by RHEB and inhibition by PRAS40. *Nature*. 2017;552(7685):368–373.
36. Ha ZL, Yu ZY. Downregulation of miR-29b-3p aggravates podocyte injury by targeting HDAC4 in LPS-induced acute kidney injury. *Kaohsiung J Med Sci*. 2021;37(12):1069–1076.
37. Li YZ, Peng X, Ma YH, Li FJ, Liao YH. Matrine suppresses lipopolysaccharide-induced fibrosis in human peritoneal mesothelial cells by inhibiting the epithelial-mesenchymal transition. *Chin Med J (Engl)*. 2019;132(6):664–670.
38. Le LT, Swingler TE, Crowe N, et al. The microRNA-29 family in cartilage homeostasis and osteoarthritis. *J Mol Med (Berl)*. 2016;94(5):583–596.
39. Li Z, Yi N, Chen R, et al. miR-29b-3p protects cardiomyocytes against endotoxin-induced apoptosis and inflammatory response through targeting FOXO3A. *Cell Signal*. 2020;74:109716.
40. Eken SM, Christersdottir T, Winski G, et al. miR-29b mediates the chronic inflammatory response in radiotherapy-induced vascular disease. *JACC Basic Transl Sci*. 2019;4(1):72–82.
41. Zhao J, Ma X, Xu H. miR-29b-3p inhibits 22Rv1 prostate cancer cell proliferation through the YWHAE/BCL-2 regulatory axis. *Oncol Lett*. 2022;24(2):289.
42. Ouseph MM, Huang Y, Banerjee M, et al. Autophagy is induced upon platelet activation and is essential for hemostasis and thrombosis. *Blood*. 2015;126(10):1224–1233.
43. Zhou K, Zheng Z, Li Y, et al. TFE3, a potential therapeutic target for spinal cord injury via augmenting autophagy flux and alleviating ER stress. *Theranostics*. 2020;10(20):9280–9302.
44. Bartel DP. MicroRNAs: genomics, biogenesis, mechanism, and function. *Cell*. 2004;116(2):281–297.
45. Sekiya Y, Ogawa T, Yoshizato K, Ikeda K, Kawada N. Suppression of hepatic stellate cell activation by microRNA-29b. *Biochem Biophysic Res Commun*. 2011;412(1):74–79.
46. Wang B, Komers R, Carew R, et al. Suppression of microRNA-29 expression by TGF-β1 promotes collagen expression and renal fibrosis. *J Am Soc Nephrol*. 2012;23(2):252–265.
47. Wang L, Yang L, Zhuang T, Shi X. Tumor-derived exosomal miR-29b reduces angiogenesis in pancreatic cancer by silencing ROBO1 and SRGAP2. *J Immunol Res*. 2022;2022:4769385.
48. Yan T, Huang L, Yan Y, Zhong Y, Xie H, Wang X. Bone marrow mesenchymal stem cell-derived exosome miR-29b-3p alleviates UV irradiation-induced photoaging in skin fibroblast. *Photodermatol Photoimmunol Photomed*. 2023;39(3):235–245.
49. Li N, Cui J, Duan X, Chen H, Fan F. Suppression of type I collagen expression by miR-29b via PI3K, Akt, and Sp1 pathway in human Tenon's fibroblasts. *Invest Ophthalmol Vis Sci*. 2012;53(3):1670–1678.
50. Subramanian M, Rao SR, Thacker P, Chatterjee S, Karunagaran D. MiR-29b downregulates canonical Wnt signaling by suppressing coactivators of β-catenin in human colorectal cancer cells. *J Cel Biochem*. 2014;115(11):1974–1984.
51. Larabi A, Barnich N, Nguyen HTT. New insights into the interplay between autophagy, gut microbiota and inflammatory responses in IBD. *Autophagy*. 2020;16(1):38–51.
52. Yao RQ, Ren C, Xia ZF, Yao YM. Organelle-specific autophagy in inflammatory diseases: a potential therapeutic target underlying the quality control of multiple organelles. *Autophagy*. 2021;17(2):385–401.
53. Cheng P, Xie J, Liu Z, Wang J. Aldose reductase deficiency inhibits LPS-induced M1 response in macrophages by activating autophagy. *Cell Biosci*. 2021;11(1):61.
54. Ryu JK, Kim SJ, Rah SH, et al. Reconstruction of LPS transfer cascade reveals structural determinants within LBP, CD14, and TLR4-MD2 for efficient LPS recognition and transfer. *Immunity*. 2017;46(1):38–50.
55. Lee JW, Nam H, Kim LE, et al. TLR4 (toll-like receptor 4) activation suppresses autophagy through inhibition of FOXO3 and impairs phagocytic capacity of microglia. *Autophagy*. 2019;15(5):753–770.

Investigative Ophthalmology & Visual Science

56. Zhou M, Xu W, Wang J, et al. Boosting mTOR-dependent autophagy via upstream TLR4-MyD88-MAPK signalling and downstream NF-κB pathway quenches intestinal inflammation and oxidative stress injury. *EBioMedicine*. 2018;35:345–360.
57. Fang W, Bi D, Zheng R, et al. Identification and activation of TLR4-mediated signalling pathways by alginate-derived guluronate oligosaccharide in RAW264.7 macrophages. *Sci Rep*. 2017;7(1):1663.
58. Gao J, Wei B, de Assuncao TM, et al. Hepatic stellate cell autophagy inhibits extracellular vesicle release to attenuate liver fibrosis. *J Hepatol*. 2020;73(5):1144–1154.
59. Zhang XW, Zhou JC, Peng D, et al. Disrupting the TRIB3-SQSTM1 interaction reduces liver fibrosis by restoring autophagy and suppressing exosome-mediated HSC activation. *Autophagy*. 2020;16(5):782–796.
60. Yu FS, Yin J, Xu K, Huang J. Growth factors and corneal epithelial wound healing. *Brain Res Bull*. 2010;81(2-3):229–235.
61. Jia LF, Huang YP, Zheng YF, et al. miR-29b suppresses proliferation, migration, and invasion of tongue squamous cell carcinoma through PTEN-AKT signaling pathway by targeting Sp1. *Oral Oncol*. 2014;50(11):1062–1071.
62. Nasiri-Ansari N, Nikolopoulou C, Papoutsi K, et al. Empagliflozin attenuates non-alcoholic fatty liver disease (NAFLD) in high fat diet fed ApoE((-/-)) mice by activating autophagy and reducing ER stress and apoptosis. *Int J Mol Sci*. 2021;22(2):818.
63. Saber SH, Ali HEA, Gaballa R, et al. Exosomes are the driving force in preparing the soil for the metastatic seeds: lessons from the prostate cancer. *Cells*. 2020;9(3):564.